



ISSN: 2800-1729

Edition : Vol 4. Num 1 (2025)

Biopolymer Applications Journal



Editor in chief:

Pr. HAMMICHE Dalila



UNIVERSITÉ ABDERRAHMANE MIRA - BEJAIA
FACULTÉ DE TECHNOLOGIE

Table of content

Lisa KLAAI, Dalila HAMMICHE

Adsorption of methylene blue dyes in aqueous medium by Polylactic Acid/Olive Husk flours biocomposites.

Vol 4, N°1, 2025, pp. 01-04

Bahia BOUBEKEUR, Dehbia NOUARI, Hadjer BENALI, Naima BELHANECHÉ

Aging of the composite material in different environments.

Vol 4, N°1, 2025, pp. 05-09

Badrina DAIRI, Nadira BELLILI, Nassima DAIRI, Achouak LEBIOD

Study of the effect of the introduction of plant fibers on the properties of composites.

Vol 4, N°1, 2025, pp. 10-16

Aicha DEHANE, Lisa KLAAI, Dalila HAMMICHE, Balbir Singh KAITH

Comparative analysis of extracted chitosan versus commercial one: Physiochemical effects of extraction.

Vol 4, N°1, 2025, pp. 17-19

Aghilas HANNOU, Rabah FERHOUM, Marzak ZEROUKII, Madjid ALMANSBA

Polymethyl Methacrylate UV aging: numerical modeling and experimental validation.

Vol 4, N°1, 2025, pp. 20-24

Adsorption of methylene blue dyes in aqueous medium by polylactic acid/olive husk flours biocomposites

Lisa KLAAI^{1,*}, Dalila HAMMICHE¹

¹Université de Bejaia, Faculté de Technologie, Laboratoire des Matériaux Polymères Avancés (LMPA), Route de Targa-Ouzemmour, Bejaia 06000, Algérie

Corresponding author*: lisa.klaai@univ-bejaia.dz

Received: 10 September, 2024; Accepted: 07 October, 2024; Published: 18 January, 2025

Abstract

The dyes present in the waste from the textile industry represent a real danger for humans and their environment, due to their low biodegradability and their toxicity. For this, new eco-designed technologies for the treatment of polluted water. Several materials have been used in photocatalysis.

This work aims to degrade the dye Methylene Blue (BM) by photo catalysis-solar using polylactic acid /Olive husk flours biocomposites materials.

The degradation of this substance was followed by UV/Visible spectrophotometry, and the best result was obtained by the composite material loaded with 30% olive husk

Keywords: Biocomposite, Dyes degradation, Methylene Blue (BM), Polylactic Acid, photo catalysis-solar.

I. Introduction

Synthetic dyes represent a relatively large group of organic chemical compounds used in our daily life [1, 2]. Global production is estimated to be about 700,000 tons/year, of which 140,000 tons are released into effluents during various applications and manufacturing stages because of wrong or negligent discharges [3,4]. If not adequately treated, these effluents, composed of surfactants, biocide compounds, solid suspensions, dispersal and mooring agents, dyes, and metal traces, are toxic to most living organisms [5,6]. Their heterogeneous composition makes it difficult to reach pollution levels less or equal to those imposed by environmental standards when adopting the traditional treatments commonly used in municipal wastewater plants [7].

One of the primary concerns of water pollution is the dye contamination of wastewater from the textile industry, which is a significant chemical, physical, and aesthetical pollutant [8]. Eutrophication and disturbance of aquatic life (e.g., limiting access to sunlight and oxygen) presents a potential environmental danger. Possible bioaccumulation also represents a further threat, affecting human health and the environment. Several techniques can be used for pollution treatment, and adsorption has been commonly considered a reliable, versatile, and efficient option [9]. When applying this technique, the adsorbents that have been most adopted for use are commercial activated carbons, which are usually expensive despite their proven efficiency. In some cases, their use produces delayed pollution, representing an additional environmental threat [10, 11]. For these reason, in recent years different biodegradable polymers have been studied, to be used as media filters and applied at an

industrial level depending on the manufacturing process [12–14]. Polymers such as polyurethane, polyacrylonitrile, polyvinylidene fluoride, polyvinyl chloride (PVC)/PU, polycarbonate, silk, polyimide and PLA poly (lactic acid) [15] have been used in the production of air filtration media, the latter having good biodegradable properties. Lactic acid is a precursor of poly (lactic acid) (PLA), with biodegradable characteristics [16].

Several studies have been carried out on the preparation of composites based on PLA for application as a water vapor barrier, antimicrobial properties [17], thermal properties [18] and mechanical properties [19–21].

The aim of this study is to determine the effect olive husk flours integrated to PLA in the adsorption of methylene blue, and the possibility to use this designed material to produce a new filter medium in health and environmental areas. For this purpose, to ensure flours dispersion, melt extrusion was used for the fabrication of poly (lactic acid) (PLA) and olive husk flours (10, 20, and 30 wt %) polymer biocomposites.

II. Material and methods

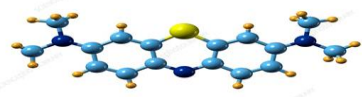
The PLA used is in the form of pellets, obtained by Nature Works in the grade of 2003D. It has a density of 1.24g/cm³, Tg between 55 and 60°C and Tm between 145 and 210 °C.

Olive husk (OH) was collected at a modern oil mill in Bejaia, Algeria.

The vegetable filler used is common reed flour (OHF). Common reed flour obtained after sieving having an average particle diameter equal to 80µm.

The dye investigated in this work was methylene blue (MB: C₁₆H₁₈N₃SCl), its physico-chemical properties are detailed in Table 1.

Table 1: Physico-chemical properties of methylene blue (MB) [21].

Dye	Methylene blue
Structure	<chem>C16H18N3SCl</chem>
Chemical formula	
Molar mass (g/mol)	319.85
Maximum wavelength λ_{\max} (nm)	664

II.1. Preparation of composites

Composite samples of PLA/OHF was compounded by melt mixing using extrusion type 2005 micro-compounder DSM Xplore model (Screw temperature is set at 180°C; the speed of rotation is 100 rpm and a residence time of 8 min), followed by compression molding of the Carver type (Press temperature is at 180°C, first preheated for 5 min and pressed for 8 min under a load of 300 KN).

The proportions of the PLA/OHF mixtures used respectively are: 90/10, 80/20, 70/30.

II.2. Photo-catalytic evaluation

The mass concentration of aqueous solutions containing the molecule to be degraded was around 50 mg/L for MB. The rate of PLA/OHF photocatalyst degradation (10.20 and 30wt% flours) under solar light irradiation is evaluated for the dye.

Practically, 25 mg of the powder of different composite materials are dispersed in an aqueous solution of volume 50 ml containing the dye. The mixture is put in a glass crystallizer covered with self-adhesive plastic film. Before the irradiation of the solution by the solar, the medium is placed under magnetic stirring in the dark for 50 minutes, in order to reach the adsorption equilibrium. After a time equal to 50 min, the concentration is almost stabilized regardless of the adsorption-desorption equilibrium couple. After 50 min of adsorption, the solution was exposed to the solar light and the chronometer starts counting time. During the photocatalysis activity, samples of 2 ml were taken, at increasing time intervals, the sample was Centrifuged at 3000 rpm for 5 min and then filtered to remove the catalyst. The resulting filtrate was analyzed by the UV spectrophotometer.

The percentage of adsorption efficiency was calculated according to Equation (1):

$$\% \text{ Adsorption} = \left(\frac{A_0 - A_t}{A_0} \right) * 100 \quad (1)$$

Where, A_0 is the absorbance of initial MB; A_t is the absorbance of the solution after illumination at time t .

II.3. Characterization

The optical properties of prepared MB/Composites were investigated using UV-Visible absorption spectroscopy (UVmini-1240, SHIMADZU) at a maximum absorption wavelength of $\lambda_{\max} = 664$ nm.

The adsorption tests were repeated twice to assess the reproducibility of the results, with the average values considered.

III. Results and discussion

III.1. Photo catalytic activity

a. Photodegradation of methylene blue (MB)

Methylene Blue (BM) is a blue dye characteristic of textile pollutants. Its absorbance spectrum is shown in Figure I.

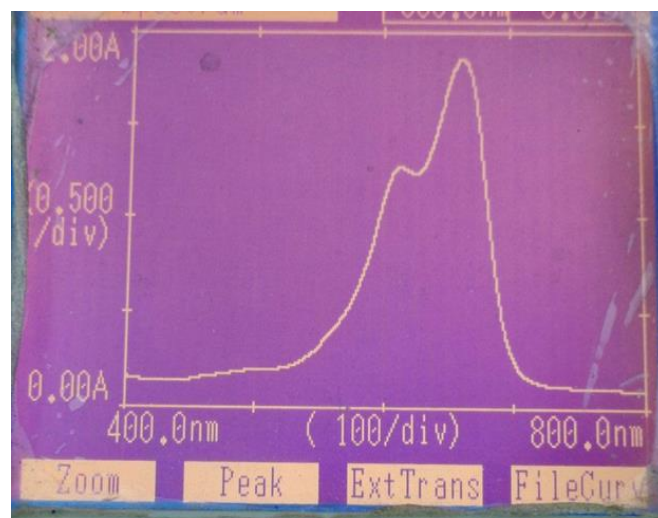


Figure 1: Absorption spectrum of photo-degraded methylene blue (MB) without catalyst

The evolution of the absorbance of the methylene blue (BM)/PLA/OHF (10wt %), PLA/OHF (20wt %) and PLA/OHF (30wt %) solution as a function of the solar irradiation time are given in Figure 2. All photo-catalytic processes were carefully monitored by measuring the maximum absorption bands of this dye at predetermined time intervals. A reduction in the maximum absorption band in MB was noticed when the exposure time to solar irradiation was increased.

In the presence of photocatalyst PLA/OHF (10wt %), PLA/OHF (20wt %) and PLA/OHF (30wt %) show removal of MB to some extent which is attributed to fiber adsorption [22]. The porous fiber of OHF has proven to be effective, where the porous structure of fibers allows the contact of OHF with MB [23].

All composite fibers with OHF show higher MB removal, where the adsorption under dark condition resulted at MB removal of 10 %, 13.7 %, and 17.7 % for OHF(10 wt%)/PLA, OHF(20 wt%)/ PLA, and OHF(30 wt%)/PLA, respectively.

In this study, the usage of solar light source was performed to observe the maximum ability of synthesized photocatalyst composite. Under this condition, the composite of OHF (30 wt %) /PLA shows the excellent removal of MB, where 70 % MB was removed after 40 min irradiation, and 88 % MB removed after 50min of irradiation. While the composite of OHF (10 wt %) /PLA showed lower degradation of MB at 72.5 % removal after 50 min of irradiation.

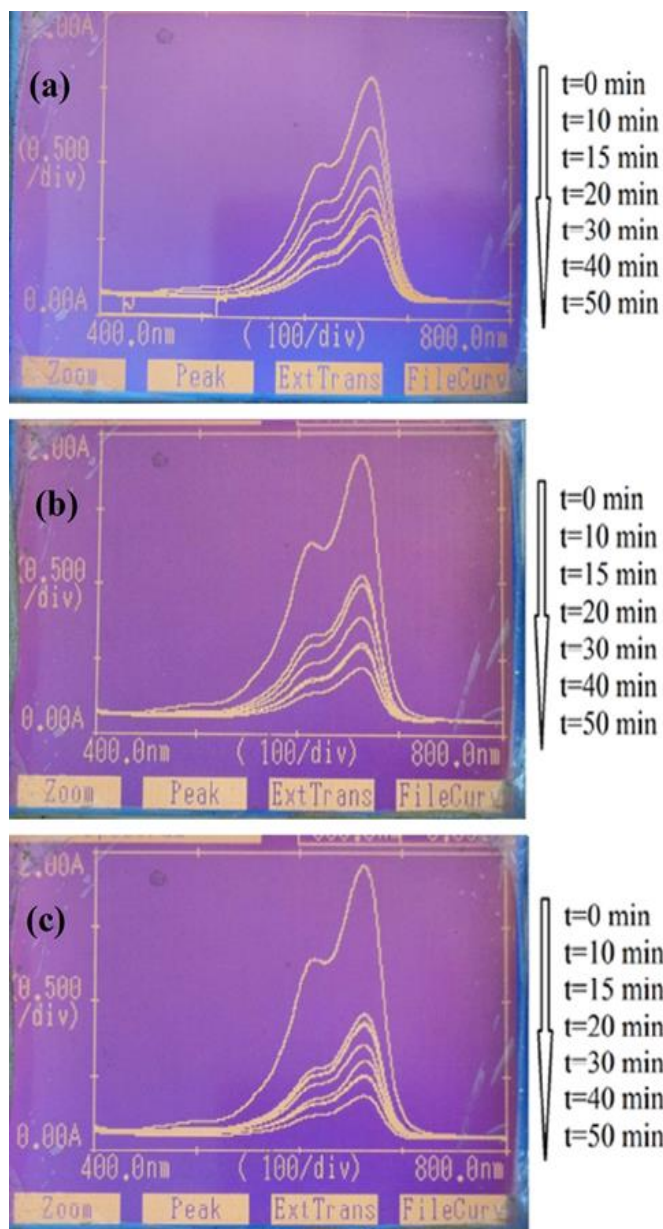


Figure 2: Absorbance profile of MB from sample taken at certain time interval by using: (a) PLA/OHF (10wt %), (b) PLA/OHF (20wt %) and (c) PLA/OHF (30wt %).

The results obtained at the end of study of Aarfane et al [24], made it possible to conclude that after 20 minutes of agitation, the BM elimination yield of aqueous solutions at 25 mg/L can reach 96% and 89% respectively during the use of the palm bark and the sugar cane bagasse. So these two plant substrates have proven to be natural supports with an affinity of significant adsorption with regard to MB. The abundance of these plant substrates can provide low -cost adsorption materials which can possibly contribute to the processing of textile effluents. In the study of Ho et al [25], porous polylactic acid (PLA) fibers were utilized as photocatalyst support using electrospinning technique to synthesis the fibers. The cadmium sulfide (CdS) was embedded in fibers at the amount of 1 wt%, 3 wt%, and 5 wt% as photocatalyst agent with absorption in visible light range. The photodegradation was performed under low-powered halogen

lamp, with 90 % removal of methylene blue (MB) after 10 hours of irradiation using CdS (3 wt %) /PLA fibers. This result shows higher performance in comparison with PLA and CdS which could only remove 57 % and 65 % of MB, respectively.

IV. Conclusions

In this work, Olive Husk flours (10, 20, and 30 wt %) integrated to PLA was used to determine its effect in the adsorption of methylene blue under solar light irradiation, and the possibility to use this designed material to produce a new filter medium in health and environmental areas.

At predetermined time of solar irradiation, a reduction in the maximum absorption band in MB was noticed when the exposure time to solar irradiation was increased.

The composite of OHF (30 wt %) /PLA shows the excellent removal of MB, where 70 % MB was removed after 40 min irradiation, and 88 % MB removed after 50min of irradiation. While the composite of OHF (10 wt %) /PLA showed lower degradation of MB at 72.5 % removal after 50 min of irradiation.

References

- [1] I.Z. Aksu, S. Ertuğrul, G. Dönmez . Methylene Blue biosorption by *Rhizopus arrhizus*: Effect of SDS (sodium dodecylsulfate) surfactant on biosorption properties. *Journal of chemical engineering*. 2010, 158, 474–481, (2010)
- [2] A.M.M. Vargas, A.L. Cazetta, M.H. Kunita, T.L. Silva, V.C. Almeida. Adsorption of methylene blue on activated carbon produced from flamboyant pods (*Delonix regia*): Study of adsorption isotherms and kinetics models. *Journal of chemical engineering*. 168, 722–730, (2011)
- [3] P.A. Carneiro, R. Nogueira, M.V.B. Zanoni. Homogeneous photodegradation of CI reactive blue 4 using a photo-Fenton process under artificial and Solar irradiation. *Dye. Pigment*. 74, 127–132. (2007)
- [4] V.K. Gupta, R. Kumar, A. Nayak, T.A. Saleh, M.A. Barakat. Adsorptive removal of dyes from aqueous solution onto carbon nanotubes: A review. *Advances in Colloid and Interface Science* 193, 24–34, (2013)
- [5] E.A. El-Sharkawy, A.Y. Soliman, K.M. Al-Amer. Comparative study for the removal of methylene blue via adsorption and photocatalytic degradation. *Advances in Colloid and Interface Science*. 310, 498–508, (2007)
- [6] V.K. Garg, M. Amita, R. Kumar, R. Gupta. Basic dye (methylene blue) removal from simulated wastewater by adsorption using Indian Rosewood sawdust: A timber industry waste. *Dye. Pigment*. 63, 243–250, (2004)
- [7] H. Zollinger. *Colour Chemistry-Synthesis, Properties of Organic Dyes and Pigments*; VCH Publishers: New York, NY, USA, 1987, 92–100, (1987)
- [8] V. Gupta, S.I. Ali, V. Saini. Removal of rhodamine B, fast green, and methylene blue from wastewater using red mud, an aluminium industry waste. *Industrial &*

- Engineering Chemistry Research. 43, 1740–1747, (2004)
- [9] P. Nigam, G. Armour, I.M. Banat, D. Singh, R. Marchant. Physical removal of textile dyes & solid-state fermentation of dye-adsorbed agricultural residues. *Bioresource technology*. 72, 219–226, (2000)
- [10] A.R. Binupriya, M. Sathishkumar, D. Kavitha, K. Swaminathan, S.E. Yun, S.P. Mun, Experimental and Isothermal Studies on Sorption of Congo Red by Modified Mycelial Biomass of Wood Rotting Fungus. *Clean Soil Air Water*, 35, 143–150, (2007)
- [11] D.S. Malik, C.K. Jain, A.K. Yadav. Removal of heavy metals from emerging cellulosic low-cost adsorbents: A review. *Applied water science*. 7, 2113–2136, (2017)
- [12] R. Kishor, Bharagava, G. Saxena, Industrial Wastewaters. In *Recent Advances in Environmental Management*; Informa: London, UK, 1–25, (2018)
- [13] J. Zhao, Q. Shi, S. Luan, L. Song, H. Yang, H. Shi, J. Jin, X. Li, J. Yin, P. Stagnaro, Improved biocompatibility and antifouling property of polypropylene non-woven fabric membrane by surface grafting zwitterionic polymer. *Journal of Membrane Science*. 369, 5–12, (2011)
- [14] S.P. Dharupaneedi, S.K. Nataraj, M. Nadagouda, K.R. Reddy, S.S. Shukla, T.M. Aminabhavi, Membrane-based separation of potential emerging pollutants. *Separation and Purification Technology*. 210, 850–866, (2019)
- [15] D. Zaarei, A.A. Sarabi, F. Sharif, S.M. Kassirha. Structure, properties and corrosion resistivity of polymeric nanocomposites coatings based on layered silicates. *Journal of Coatings Technology and Research*. 5, 241–249, (2008)
- [16] J.W. Rhim, S.I. Hong, C.S. Ha. Tensile, water vapor barrier and antimicrobial properties of PLA/nanoclay composite films. *LWT* 2009, 42, 612–617, (2009)
- [17] M. Iturrondobeitia, T. Guraya, A. Okariz, V. Srot, P.A. an Aken, J. Ibarretxe, M.I. Ellacuria. Quantitative electron tomography of PLA/clay nanocomposites to understand the effect of the clays in the thermal stability. *Journal of applied polymer science*, 134, (2017)
- [18] M. Iturrondobeitia, J. Ibarretxe, A. Okariz, P. Jimbert, R.F. Martinez, T. Guraya. Semi-automated quantification of the microstructure of PLA/clay nanocomposites to improve the prediction of the elastic modulus. *Polymer testing*. 66, 280–291, (2018)
- [19] S.Y. Lee, Y.X. Xu, M.A. Hanna. Tapioca Starch-poly (lactic acid)-based Nanocomposite Foams as Affected by Type of Nanoclay. *International polymer processing*. 22, 429–435.(2007)
- [20] P. Krishnamachari, J. Zhang, J. Lou, J. Yan, L. Uitenham. Biodegradable Poly(Lactic Acid)/Clay Nanocomposites by Melt Intercalation: A Study of Morphological, Thermal, and Mechanical Properties. *International Journal of Polymer Analysis and Characterization*. 14, 336–350, (2009)
- [21] Y. Chen, G.-F. Huang, W.-Q. Huang, B. S. Zou, A. Pan. Enhanced visible-light photoactivity of La-doped ZnS thin films. *Applied Physics*, 108, 895-900, (2012)
- [22] J.O. Quansah, T. Hlaing, F.N. Lyonga, P.P. Kyi, S.H. Hong, C.G. Lee, S.J. Park, . Nascent Rice Husk as an Adsorbent for Removing Cationic Dyes from Textile Wastewater. *Applied science letters*. 10, 3437 (2020)
- [23] X. Cheng, Y. Jia, J. Qiang, L. Wen, C. Zhang, X. Yang, and L. Liang, A facile method to prepare CdS/polymer nanocomposite fibers for the photodegradation of methylene blue under sunlight *Journal of Polymer Science and Engineering*, 37, 107 (2017).
- [24] A. Aarfane , S. Tahiri , A. Salhi , G. El Kadiri Boutchich , M. Siniti , M. Bensitel , B. Sabour , M. El Krati. Adsorption of methylene blue and Red195 dyes in aqueous medium by palm bark and sugarcane bagasse: kinetic and thermodynamic study. *Journal of Materials and Environmental Science*. 6 (10), 2944-2957, (2015)
- [25] C.S Ho, N.H.Z. Abidin, M.W. Nugraha, N.S. Sambudi, A. Fathilah, M.D.H. Wirzal, L.D. Kasmiarno, S.A Adli. Electrospun Porous Polylactic Acid Fibers Containing CdS for Degradation of Methylene Blue. *Fibers and Polymers*. 21(6), 1212-1221, (2020)

Aging of the composite material in different environments

Bahia BOUBEKEUR^{1,2*}, Dehbia NOUARI², Hadjer BENALI², Naima BELHANECHÉ²

¹Environmental Science and Technology laboratory / UMBB, Boumerdes, Algeria

²Environmental Science and Technology laboratory /ENP, Alger, Algérie

Corresponding author*: b.boubekour@univ-boumerdes.dz

Received: 22 September, 2024; Accepted: 25 October, 2024; Published: 20 January, 2025

Abstract

The present work concerns the study of aging a new biodegradable material by mixing the poly lactic acid (PLA), thermoplastic biodegradable, with a low density in the presence of compatibilist PE-GMA in a different environment. The sample formulations LDPE/PLA/PE-GMA (20/80/5; 0/100/0; 100/0/0) are tested in soil and water over time. The aged samples are characterized (by mass loss, pH, and infrared spectroscopy). The results show that the mass loss of blend LDPE/PLA/PE-GMA is 24% after 5 weeks in water at 60°C. The pH value decreases over time. A negligible amount of mass loss in the soil is observed with a pH of 5 and ambient temperature. All results are confirmed by analysis of Infrared Spectroscopy.

Keywords: chemical hydrolysis, low-density polyethylene, polylactic acid, soil

I. Introduction

Poly(lactic acid) (PLA) is the most important biodegradable polyester with wide applicability in many fields, such as biomedical. PLA has good biocompatibility, and good physical properties such as high strength and high modulus, however, PLA is very brittle [1]. PLA is commonly used as a component of biodegradable materials in pharmaceutical, biomedical, and environmental applications [2]. Density Polyethylene is one of the current thermoplastics that has a higher elongation at break than PLA but is not degradable for this reason, biodegradable polymers like polylactic acid, acorn-based polymer, have been the subject of many studies during the past decade[3].

The increasing manufacturing of green materials in recent years is related to the preoccupation with environmental protection. For that reason, researchers have been oriented toward the elaboration of new environment-friendly biocomposite materials either based on polymers originating from petroleum such as no biodegradable PE, PP, or the plant world (PLA, PBAT...).

Among the biodegradable polymers, polylactic acid (PLA) is increasingly used because it is a biodegradable, biocompatible polymer that can be produced from renewable resources, has low cost, high specific strength, and can substitute polymers derived from petroleum (PP, PE, etc) [4-7]. Protecting the environment means reducing the waste generated by the significant consumption of common thermoplastics such as polyethylene and polypropylene, 40% of which is intended for packaging. To this end, attention has been focused on biodegradable polymers derived from renewable resources such as polylactic acid (PLA). The development of new materials, based on polymer blends, presents an economic and environmental advantage.

An alternative is to minimize the amount of non-degradable polymer by biodegradable substitutes, the goal is to have new materials, both biodegradable and with an affordable price.

As part of this study, we are interested in the behavior of a material PEBD/PLA/PE-GMA, (20/80/5), (100/0/0), and 0/100/0) in soil and water.

II. Material and methods

We used samples already developed see [8]. The samples are cut into a square shape measuring (1cm x 1cm) numbered and steamed at 105°C until constant weight then they are weighed.

Provide sufficient detail to allow the work to be reproduced. Methods already published should be indicated by a reference: only relevant modifications should be described.

Figure 1:



Figure 1: Samples of material

The used soil is taken from the public dump of Mikla town of Tizi Ouzou Algeria. It is dried in the open air for 10 days, crushed, and sifted. We've determined soil composition and characteristics. The working method is illustrated in Figure 2.

II.1 Hydrolysis

Aging by hydrolysis of samples in distilled water was studied at different temperatures: 45°C and 60°C. The samples of the

LDPE/PLA/PEG-GMA formulations (20/80/5; 0/100/0; 100/0/0) thus prepared are placed in glass jars each filled with 150 ml of distilled water pH= 7.8 well closed at the chosen temperatures, the whole is immersed in the water bath. The duration of aging is spread over 5 and 4 weeks respectively. Three samples were taken each week.

II.2 Biodegradation of material in soil

Aging in the soil is studied in different environments. The samples of the LDPE/PLA/PEG-GMA formulations (20/80/5; 0/100/0; 100/0/0) thus prepared are buried in the ground:

- Anaerobic at room temperature,
- Aerobic at room temperature,
- Thermal at a temperature of 60°C.

Watering is done with distilled water with a pH equal to 7.8 and acidic tap water with a pH equal to 5 in the three studied cases above. Aging took place over 2 months:

Three samples were taken every 15 days for each formulation.

Water is added to each container to compensate for the water loss and maintain a fixed humidity level.

The evaluation of biological and hydrothermal aging was determined by the evolution of:

- The loss of mass, as a function of time.
- pH of the medium as a function of time,
- Characterization of spectral FTIR of samples.

II.3 Mesure de la perte de masse (gravimétrie)

Après le lavage ; les échantillons, ont été séchés dans une étuve à température de 105°C puis pesés, plusieurs fois afin d'obtenir une masse constante.

La perte de masse a été calculée pour chaque échantillon à l'aide d'une balance analytique de; selon la formule suivante:

$$\text{Perte de masse (\%)} : \Delta m = \frac{m_t - m_0}{m_0} \cdot 100\% \quad (1)$$

m_0 : the initial mass of the sample in grams

m_t : the mass after aging in grams.

Δm : the loss of mass which gives an indication of the rate of degradation.

II.4 Evolution of pH

For hydrolysis, the pH of the water is read directly from a pH meter.

II.4 Spectral and microscopic analysis

To confirm the chemical degradation we analyzed the samples before and after chemical, and biological degradation.

(Fourier transform infrared spectroscopy) FTIR JASCO model FT/IR 4100 type A OMNIC.

III. Results and discussion

III.1 Hydrolysis

The results of the loss weight of polymers and blend are given in Figure 2,3.

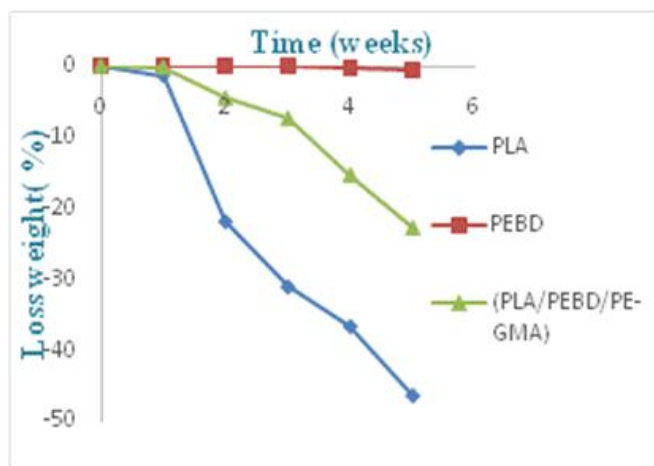


Figure 2: Lost weight in water distilled at 60°C

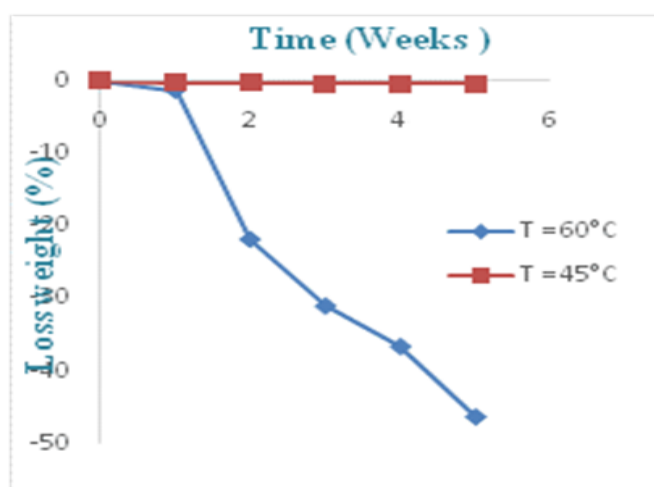


Figure 3: Loss weight of PLA in water distilled at 60°C and 45°C

The results obtained show the rate of mass loss at 60 °C is much greater than that at 45 °C. The hydrothermal degradation of the LDPE/PLA/PE-GMA mixture occurred but remained lower than that of PLA.

According to Figures 4,5 and 6, there is a strong decrease in pH at 60°C compared to that recorded at 45°C, moreover, the diminution in pH for PLA alone is faster and with a higher rate than that of the mixture. This decrease is explained by the migration of lactic acid from PLA. The incorporation of PLA into LDPE promotes the degradation of the produced material. PLA can absorb water, which results in the hydrolysis of ester bonds and causes the breakage of macromolecular chains [9] which confirms the loss of mass of the material

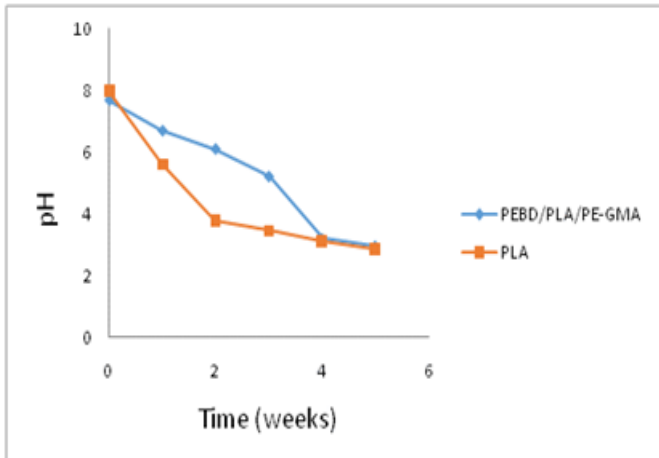


Figure 4. Evolution of pH of distilled water as a function of the aging time at temperatures 60°C.

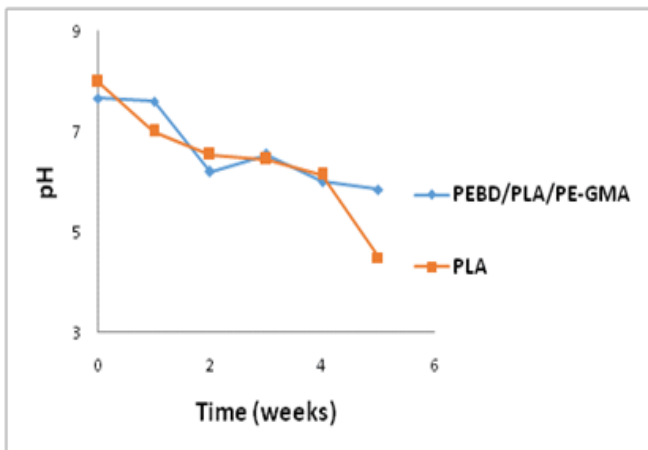


Figure 5. Evolution of pH of distilled water as a function of the aging time at temperatures 45°C.

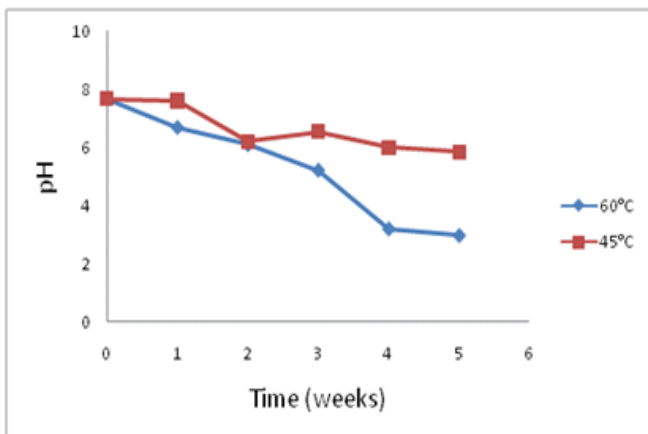


Figure 6. Evolution of pH of distilled water as a function of the aging time of the blend LDPE/PLA/PE-GMA (20/80/5) at different temperatures

III.2 Biodegradation

Soil texture is given in Table 1.

According to the results obtained, the soil has a balanced texture. Sand allows water and air to infiltrate, while clay promotes water retention

Table 1. Composition du sol

Analyse granulométrique				
Argile (%)	Limon Fin (%)	Limon. Grossier (%)	Sable Fin (%)	Sable Grossier (%)
26.15	11.55	20.75	18.40	23.15

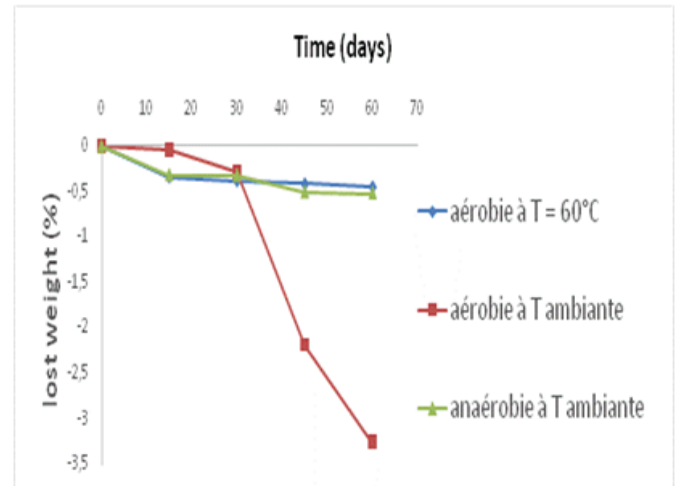


Figure 7. Loss of mass LDPE / PLA / PE-GMA (20/80/5) as a function of the aging time in soil, watered with acidulated tap water pH = 5

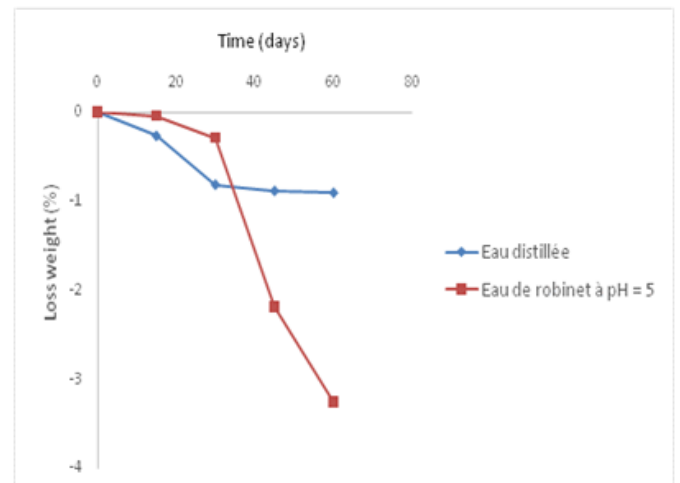


Figure 8. Loss weight of LDPE/PLA/PE-GMA aerobic soil at room temperature

The obtained results (Figure 7,8) show that the aerobic environment promotes the degradation of the LDPE/PLA/PE-GMA material (20/80/5). We note a mass loss of 3.5% and 0.4% in aerobiosis and anaerobiosis respectively in the presence of acidulated tap water at a pH of 5. But the degradation remains very low. These mass losses remain insignificant, they agree with the study carried out by Karamanlioglu et al [10] which showed an absence of degradation of PLA in the soil after twelve months at a temperature of 25 °C. Degradation of PLA in soil is difficult at low temperatures [11]. The temperature influences the degradation of PLA (figure 3) these results are consistent with the literature [12]

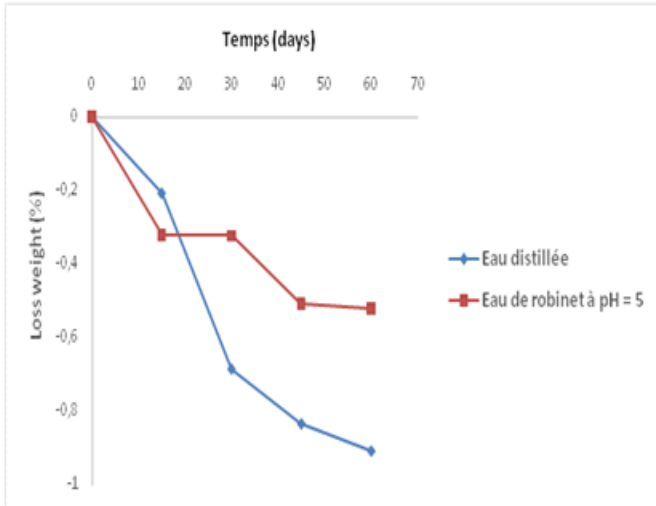


Figure 9. Loss weight of LDPE/PLA/PE-GMA anaerobic soil at room Temperature

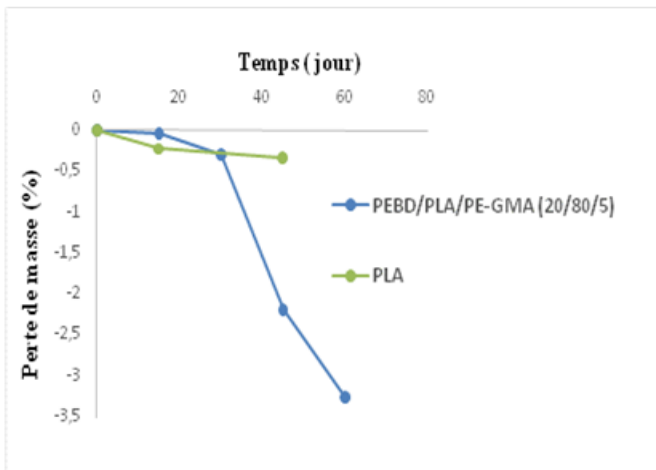


Figure 10. Loss weight of LDPE/PLA/PE-GMA and PLA aerobic soil at room T watered with acidulated tap water at pH = 5

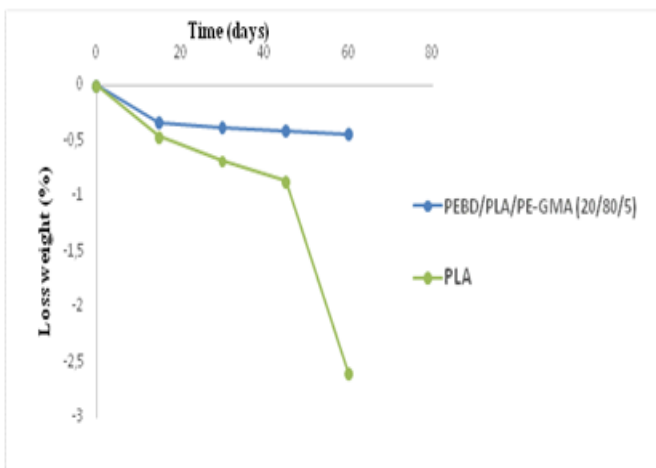


Figure 11. Loss weight of LDPE/PLA/PE-GMA and PLA aerobic soil at 60°C watered with acidulated tap water at pH = 5

The results of the mass loss illustrated by Figure 9,10 and 11 show that the high temperature promotes the degradation of PLA but this loss remains insignificant.

III.2 FTIR spectra

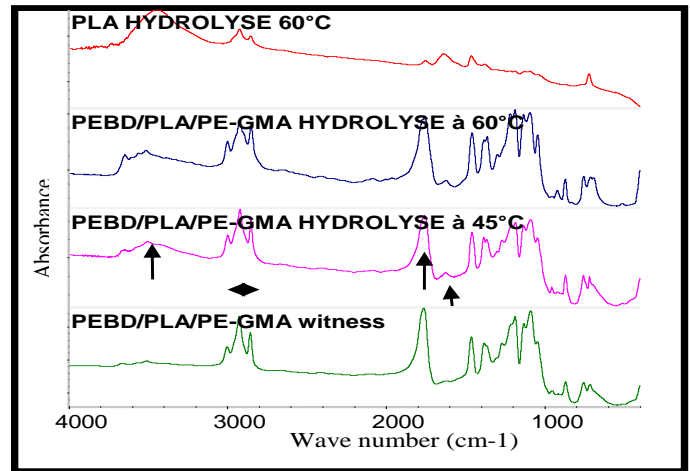


Figure 12. FTIR spectra of the different various material hydrolysis

The Figure 12. shows the LDPE / PLA / PE-GMA spectrum (20/80/5) before and after hydrolysis. The results show an increase in the intensity of the symmetrical and asymmetric CH bands (2850-3000 cm^{-1}), a broadband intensity increase between 3100-3500 cm^{-1} attributed to the hydrogen bond formation between the hydroxyl group and carboxyl groups, which is confirmed by the displacement of the carbonyl band from 1762 to 1758 cm^{-1} . The appearance of a band at 1618 cm^{-1} corresponds to the presence of water enclosed in the cracks thus formed after degradation. The increase of the band to 920 cm^{-1} corresponds to the elongation of the O-H bond of the carboxylic acids.

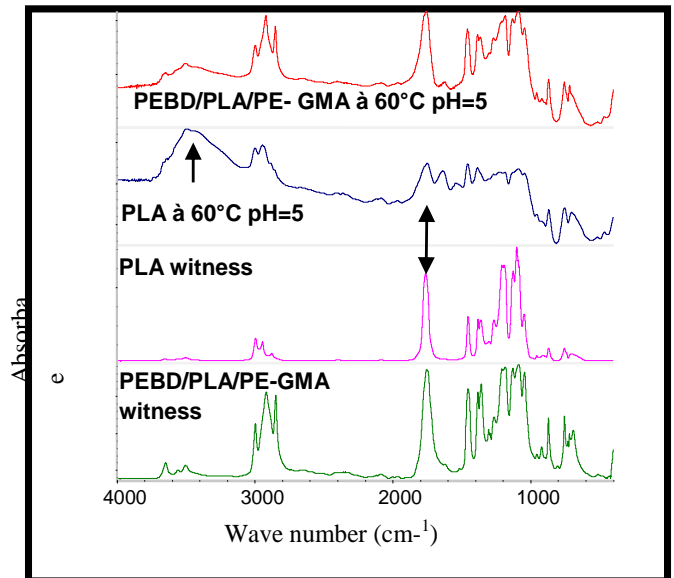


Figure 13. FTIR spectra of the various materials buried in the soil aerobic.

The spectra of the mixture before and after aging are in Figure 13. show the appearance of a wide band at 3505 cm^{-1} and that at 1620 cm^{-1} whereas the rest of the bands do not signal any specific change, however, changes in 1 The

intensity of the absorption of the 1757 cm^{-1} and 2850-2997 cm^{-1} bands thus confirming the low mass loss obtained.

IV. Conclusions

The hydrolysis of the LDPE/PLA/PE-GMA and PLA mixture takes place at a temperature above its glass transition temperature. Therefore, the pH value decreases greater at 60 °C. than at 45 °C.

Degradation of PLA in soil is difficult at low. The temperature of 60 °C. does not contribute to the degradation in the soil of the LDPE / PLA / PE-GMA material (20/80/5) in both cases: watered by distilled water or acid tap water at pH = 5. These mass losses remain insignificant.

The aerobic environment at room temperature is more favorable but the biodegradation process remains weak.

The results show that the PLA incorporation in PEBD promotes the hydrothermal of material.

The FTIR analysis shows the disappearance and appearance of bands which confirm the mass loss. The structural changes were investigated by FTIR spectroscopy. The material thus produced is much more marked by hydrolysis.

References

- [1] L.J. Chan ,Reactive Blending of Biodegradable Polymers: PLA and Starch, Journal. of polymer. and the Envirentmen, 8(1), 33-37,(200).
- [2] J.M Onyari, F. Mulaa, J. Muia, P. Shiund, Biodegradability of poly(lactic acid), preparation and characterization of PLA/Gum Arabic blends. Journal of Polymer Envirenmant 16,205-212, (2008).
- [3] M.S. Huda, LT Drzal, A.K. Mohanty, M. Misra, Effect of fiber surface treatments on the properties of laminated biocomposites from poly(lactic acid)(PLA) and kenaf fibers. Composites Science and Technology., 68(2):424-432, (2008).
- [4] D. Battegazzore ,J. Alongi. , A. Frache, Poly(lactic acid)-Based Composites Containing Natural Fillers:Thermal, Mechanical and Barrier Properties. Journal of Polyer Environment. 22,88–98 (2014).
- [5] H.S. Ki, B.H. Lee, S. Le, Enhanced interfacial adhesion, mechanical, and thermal properties of natural flour-filled biodegradable polymer bio-composites. Journal of Thermal Anaytic Calorimetrel 10, 4331–33, (2011)
- [6] M. Kowalczyk, E. Piorkowsk, Mechanical and thermal properties of PLA composites with cellulose nanofibers and standard size fibers. Journal of Composite: Part A ,42 ,1509-1514, (2011)
- [7] K.W. Kim, B.H.Lee, H.J. Kim, Thermal and mechanical properties of cassava and pineapple flour_filled PLA bio-composite, Journal of Thermal Anaytic Calorimetrel, 108,1131-113, (2012)
- [8] B. Boubekeur, N. Belhaneche-Bensemra and V. Massardier. Valorization of waste jute fibers in developing low-density polyethylene /poly lactic acid bio-based composites. Journal of Reinforced Plastic& composite, 34(8) 649–661, (2015)
- [9] S. Lee, J.W. Lee, Characterization and processing of biodegradable polymer blends of poly(lactic acid) with poly(butylenes succinate adipate). Journal of Korea-Australia. Rheolog, 17, 71-77,(2005)
- [10] M. Karamanlioglu, G.D. Robson, The influence of biotic and abiotic factors on the rate of degradation of poly(lactic) acid (PLA) coupons buried in compost and soil. Journal of Polym. Degradation and Stability, 98, 2063-2077, (2023)
- [11] A.P. Gupt, V. Kumar, New emerging trends in synthetic biodegradable polymer – Polylactide: A critique. Journal.of Euro Polymer, 43, 4053-4074, (2007)
- [12] J.polymer testing. Yun Xuan Weng. Biodegradation behavior of PBAT/PLA and their blend under soil conditions, 32(5) 918- 926, (2013)

Study of the effect of the introduction of plant fibers on the properties of composites

Badrina DAIRI ^{1,2*}, Nadira BELLILI ^{1,2}, Nassima DAIRI ^{3,4}, Achouak LEBIOD ¹

¹ Department of Process Engineering, Faculty of Technology, Skikda University 20 August – 1955 – Algeria

² Department of Process Engineering, Faculty of Technology, Laboratory of Advanced Polymer Materials (LMPA), Abderrahmane MIRA University, Béjaïa 06000, Algeria

³ Department of Industrial Chemical Technology. Institute of Technology. Akli Mohand Oulhadj University (UAMOB), Bouira. Algeria;

⁴ Department of Macromolecular Chemistry, Faculty of Chemistry, Materials Polymer Laboratory, University of Sciences and Technology Houari Boumediene USTHB, B.P. 32 El-Alia, 16111 Algiers, Algeria;

Corresponding author*: b.dairi@univ-skikda.dz

Received: 29 September, 2024; Accepted: 30 October, 2024; Published: 24 January, 2025

Abstract

To reduce the massive consumption of HDPE, which causes environmental problems, we offer biodegradable composite materials, at low cost and with low density. In this context, a study devoted to the valorization of lignocellulosic waste, a particular interest has been brought to the pistachio shell filler, as vegetable filler in the manufacture of high-density polyethylene matrix composite materials with a filler rate of 5% to 15%. The HDPE/FCP composites were initially mixed in a calendar before preparing the different sample shapes with a thickness of 2 and 3mm by compression at 190°C. The latter were characterized by various techniques: rheological, mechanical, physical tests, and morphological.

Keywords Pistachio shell fillers, High-density polyethylene, composite materials, mechanical properties, Physical properties.

I. Introduction

For several years, the emergence of concepts such as sustainable development, industrial ecology, and green chemistry has been accompanied by the development of new generations of materials. Among these materials, composites continue to evolve into high-performance and cost-effective products while meeting environmental constraints and regulatory requirements regarding recycling. Polymer matrix-based composite materials reinforced with natural fillers have garnered increasing attention due to their resulting final properties, allowing broad access to various high-value-added application areas. This is in contrast to materials derived from petroleum resources, which have environmental constraints, not to mention the limited availability of raw materials that appear to be depleting and whose cost is very high [1].

The depletion of petroleum resources, along with the rise in environmental awareness that emerged in 1990, has made various populations realize the importance of their actions on the health of our planet. It has become necessary to reduce our CO₂ emissions and waste quantities, improve recycling processes, and limit our dependence on fossil-based materials. As a result, many environmental standards have emerged in recent years to ensure the sustainability of our planet. These changes are not without impact on our daily lives and those of industries.

To better address these environmental concerns, the composite materials sector has turned to a new range of more environmentally friendly products: bio-composites. These materials have the advantage of incorporating all or part of bio-based elements and are therefore recyclable and biodegradable [2].

Incorporating natural fibers as fillers or reinforcements in plastics could also be a feasible solution to reduce cost, improve performance, reduce weight, and address environmental concerns [3].

Natural fiber-reinforced composites have, therefore, garnered increasing attention due to their low cost, low density, biodegradability, availability, ease of processing, high specific modulus, and ability to be recycled [4].

Like all natural fibers, pistachio shell fiber is hydrophilic because it is composed of lignocellulose, which contains hydroxyl groups. Therefore, it is incompatible with hydrophobic thermoplastics, which is a weak point for its use as a polymer reinforcement. It is necessary to create interactions at the interface between the polymer matrix and the fibers to avoid compromising mechanical properties. Among the numerous methods used to improve fiber-matrix compatibility, alkaline treatment [5, 6] and maleic anhydride

grafting onto the polymer matrix [7, 8] are the most commonly used.

The objective of this study is the development and characterization of a new biocomposite material based on high-density polyethylene (HDPE) reinforced with waste pistachio shell fibers.

II. Material and methods

The high-density polyethylene of type PEHD 5502, with a melt flow index of 0.35g/10min is produced by the CP2K complex (Skikda). In addition, Pistachio shell flour is used as a filler in the composite preparation.

1.1 Blend preparation

The pre-mixing of HDPE/PSF composites with different pistachio shell fiber content (5%, 10%, and 15%) is carried out in a two-roll mixer from the IQAP LAP brand at the "CP2K, Skikda" unit. The rotation speed of the two rolls is set at 32 rpm, and the temperature is maintained at 170°C. After 10 minutes, composite sheets with a thickness of 3 mm are obtained, which will be used to prepare various samples through the compression molding process.

After the mixing process, we obtained a blend of HDPE and pistachio shell flour, which we cut into small pieces (2 to 3 cm) using a manual cutter. These pieces are then placed into molds to fabricate samples in the form of dumbbells and squares, which will later be used in various characterization tests.

The films obtained from the mixing process are cut and then placed between the plates of a CARVER hydraulic press. They are heated to a temperature of 190°C for 14 minutes to prepare 3 mm thick sheets, which will be used to cut samples for various characterization tests.

Table 1: Formulations of HDPE/ PSF.

Percentage of pistachio shell fibers (%).	0	5	10	15
Parentage of HDPE (%).	100	95	90	85

2 Characterization

2.1 Tensile test

The mechanical properties at the break of the samples are measured using a TesT GmbH tensile testing machine at room temperature. The samples are cut in a dumbbell shape of type "H" with dimensions (3 x 20 x 100) mm³, following the ASTM D638 standard. The strain rate is set at 20 mm/min.

2.2 Shore D hardness test

According to the ASTM D-2240 standard, 3 mm thick plate samples are prepared using a press and then placed under the penetrator. By operating the lever arm until the steel ball or diamond cone penetrates, the value indicated by the device

can be read. Three tests are conducted at different points, and the average value is calculated.

2.3 IZOD impact test

The most common method is known by the reference IZOD (ISO 180). It is widely used in the United States (ASTM D-256), however in France, it is limited to the characterization of polystyrene (T51-911, identical to the ISO 180 standard and similar to the ASTM D256 standard).

2.4 Measurement of the fluidity index

The principle of this test is to measure the mass of molten thermoplastic material passing through a die over a certain period under the action of a defined load applied to the piston. The melt flow index, expressed in g/10min, provides information about the polymer's viscosity and, therefore, its molecular mass.

The melt flow index was determined using an extrusion plastometer (rheometer) containing a heated barrel at 190°C. A 3g sample of the material to be analyzed is introduced into the barrel, and it is pushed toward the die by a piston loaded with a weight of 2.16 kg, according to the standard: ISO 1133.

2.5 Water absorption test

The water absorption test involves drying the samples in an oven at 80°C for 24 hours. After drying, the samples are weighed using an analytical balance with a precision of 0.0001g. The samples are then immersed in distilled water at room temperature. The percentage increase in their weight is measured every 24 hours, representing their water absorption percentage during that period. Every 24 hours, the samples are removed from the water and quickly dried to remove excess surface water. Their weight is recorded within 10 to 15 seconds to minimize errors due to evaporation. The difference between the weight after each 24-hour immersion and the initial dried weight from the oven, relative to the initial dried weight, is used to determine the water absorption of the composite for that day. This value is recorded for 30 days to observe the trend in water absorption in the composites.

2.6 Determination of density

The apparent density is measured by the pycnometric method, according to the NFT 51-063 standard. Distilled water is used as the displacement solvent, ensuring the good wettability of the sample.

To study the morphology of the materials and verify the dispersion of fibers in the composite materials, optical microscopy is used to take surface photos of the obtained films. The equipment used is an optical microscope from OPTIKA Microscopes, ITALY.

III. Results and discussion

III.1 Mechanical Properties

1.1. Tensile test

- Evolution of the Stress at Break

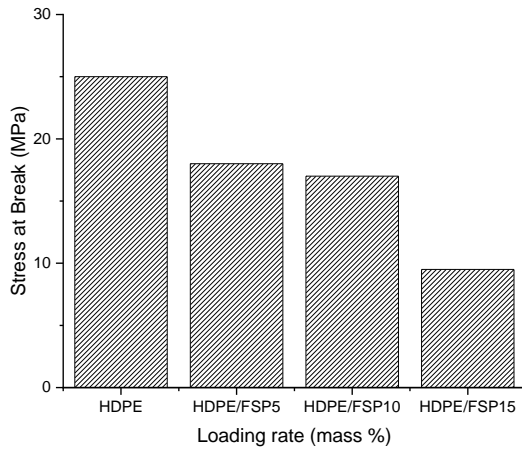


Figure 1: Evolution of the stress at break of HDPE/PSF composites as a function of the loading rate.

According to Figure 1, a decrease in the stress at break is observed with the increase in loading rate. This decrease becomes more significant as the amount of pistachio shell flour increases. These results are predictable and are consistent with many studies, such as those by S.M.B. Nachtigall et al. [9], Demir et al. [10], Khalid et al. [11], and Kaci et al. [12], who attributed this reduction to a weakening of the bond strength between the fiber and the matrix. This weakening obstructs the propagation of stress. This can be explained by the tendency of pistachio shell flour particles to cluster together, forming agglomerates that introduce heterogeneities and lead to uneven stress transfer within the matrix. As a result, the composite material becomes more brittle and fragile.

• Evolution of elongation at break

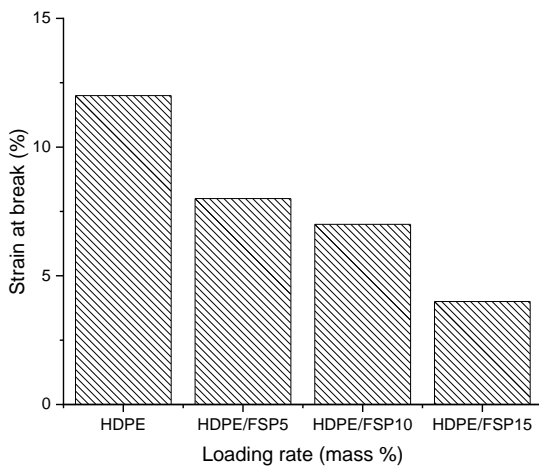


Figure 2: Variations in elongation at break of HDPE/PSF composites developed depending on the charging rate.

A significant decrease in the elongation at break is observed as the loading rate increases. Pasquini et al. [13] explained this decrease, from one perspective, by the hydrophilic nature of pistachio shell flour, which absorbs more moisture and causes swelling within the PEHD matrix, leading to material

weakening. On the other hand, it is due to the increasing volume occupied by the filler particles, which creates defects in the system and reduces the inter-chain interactions. This results in a transition from ductile to brittle behavior in the material.

• Evolution of Young's modulus

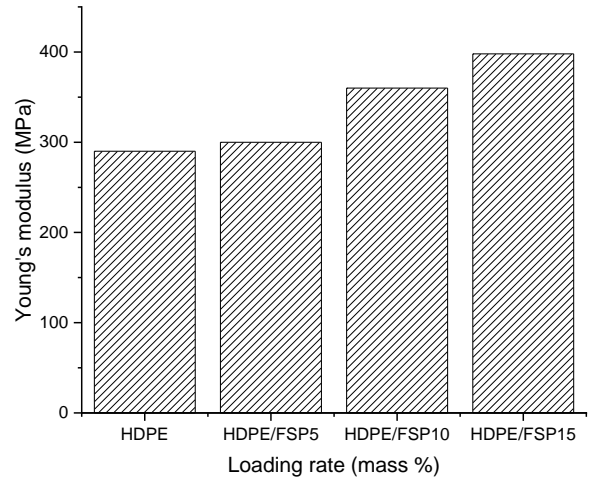


Figure 3: Variations in Young's modulus of HDPE/PSF composites as a function of rate dump.

According to Figure 3, a significant increase in the elastic modulus is observed with the increase in the loading rate. This mechanical property depends on the rigidity of the pistachio shell flour incorporated into the HDPE matrix [14].

1.2. Shore D hardness

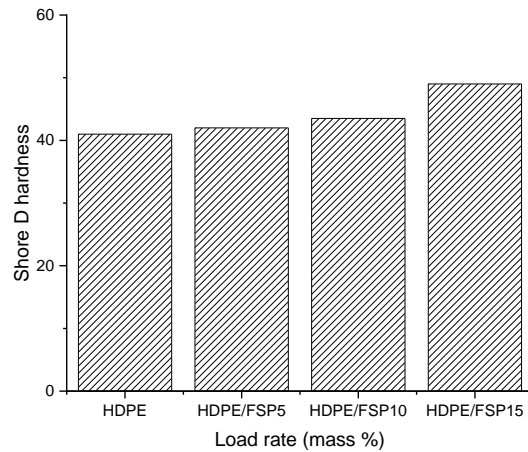


Figure 4: Evolution of the Shore D hardness of HDPE/PSF composites as a function of the charge rate.

We can observe that the incorporation of pistachio shell flour into the high-density polyethylene matrix (Figure 4) is accompanied by an increase in the hardness of the PEHD/PSF composites. This increase is more significant as the loading rate rises. These results are predictable since pistachio shell particles are composed of microfibrils of

cellulose, which are classified as hard fibers. This results in greater resistance to penetration by the durometer needle into the composite material. This outcome was confirmed by N.Stark, and R.E. Rowlands [15].

1.3. IZOD impact resistance

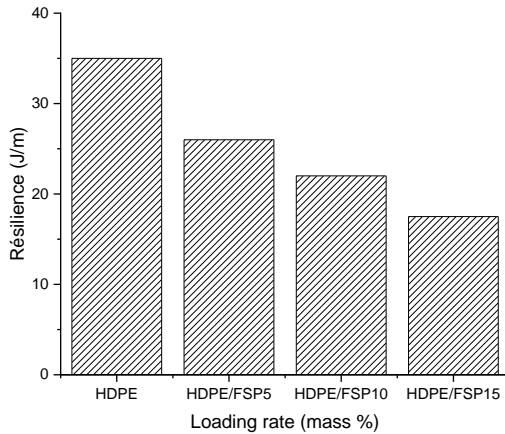


Figure 5: Evolution of the resilience of HDPE/PSF composites as a function of the rate of charge.

Figure 5 shows the variations in the impact resistance of PEHD/PSF composites as a function of the loading rate. According to this figure, the incorporation of pistachio shell flour into the PEHD matrix led to a decrease in the impact resistance of the composites. This can be explained by the incompatibility between the matrix and the pistachio shell particles reduces the adhesion between the two phases, which weakens the system, resulting in a decrease in the impact resistance of the composites. Additionally, the addition of FCP fibers, which are stiffer than PEHD, significantly increases the rigidity of the composite material, which also contributes to the reduction in impact resistance. These results are consistent with the ones presented by Petchwattana et al. [16] and Zheng et al. [17].

III.2 Rheological characterization

2.1 Melt Flow Index: MFI

Figure 6 illustrates the evolution of the melt flow index of PEHD/PSF composites as a function of the loading rate. A decrease in the melt flow index is observed with the increase in pistachio flour content. This is due to the agglomeration of pistachio shell particles, which create obstacles to the free movement of the polymer chains and prevent the flow of the material. These results are consistent with M.N. ICHAZO et al [18] ones.

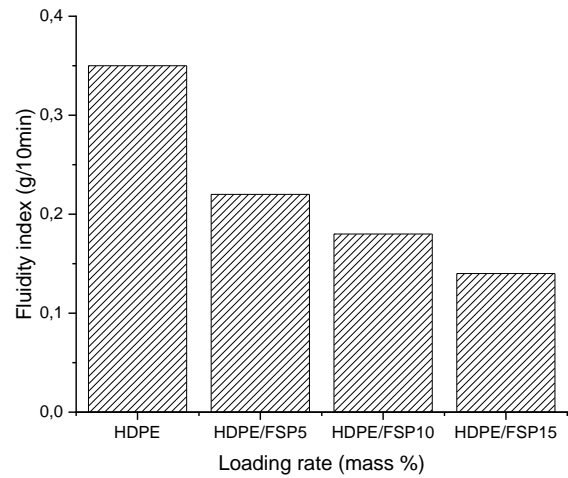


Figure 6. The fluidity index of HDPE/PSF composites evolution according to the rate dump.

Figure 6 illustrates the evolution of the melt flow index of PEHD/PSF composites as a function of the loading rate. A decrease in the melt flow index is observed with the increase in pistachio flour content. This is due to the agglomeration of pistachio shell particles, which create obstacles to the free movement of the polymer chains and prevent the flow of the material. These results are consistent with M.N. ICHAZO et al [18] ones.

III.3 Physical characterizations

3.1. Density

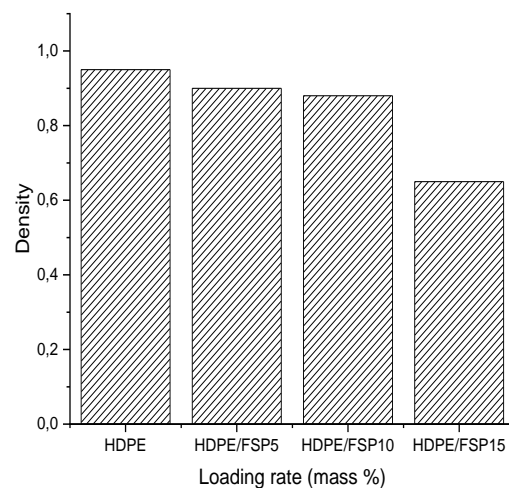


Figure 7: Evolution of the density of HDPE/PSF composites as a function of the charge rate.

The results of the density test for the composites PEHD, PEHD/PSF 5%, PEHD/PSF 10%, and PEHD/PSF 15% are presented in Figure 7. The measurement reveals that the density of pistachio shell particles is around 0.6254. In this regard, the incorporation of pistachio shell fibers into polyethylene results in composites with low density. The

density profiles of the PEHD/PSF composites decrease as the loading rate increases, ranging from 0.95 for pure PEHD to 0.89, 0.85, and 0.63 for PEHD/PSF composites with 5%, 10%, and 15% pistachio flour, respectively [19].

III.4 Water absorption test

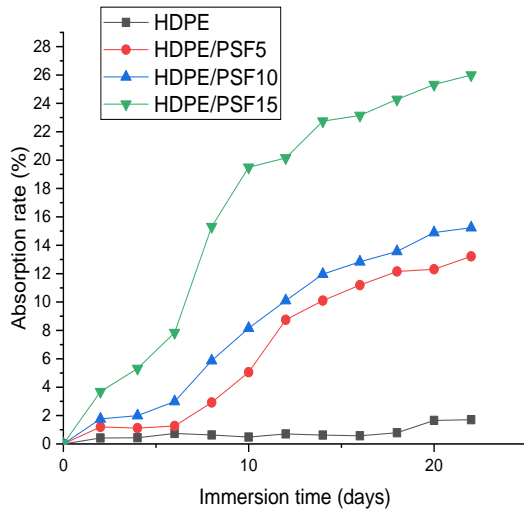


Figure 8: Evolution of the water absorption rate of HDPE/PSF composites depending on the immersion time.

We can observe an increase in the water absorption rate with immersion time and the pistachio shell flour content in the high-density polyethylene matrix. This is entirely expected since pistachio shell flour is highly rich in hydroxyl groups, which form hydrogen bonds with water molecules. Consequently, the higher the flour content, the greater the OH concentration, and thus, the water absorption rate increase. It is also noticeable that the water absorption rate of PEHD/FCP samples is initially rapid, and then slows down as time progresses until saturation is reached, where the water absorption rate becomes constant. For composites with 5%, 10%, and 15% pistachio shell flour, the maximum swelling rates are estimated at 13.7443%, 14.9659%, and 24.2842%, respectively. For virgin PEHD, a very low water absorption rate is recorded due to the non-polar nature of this polymer, which gives it hydrophobic characteristics. Water absorption is approximately 0.082% within 24 hours and does not exceed 0.033% after 15 days. These values are confirmed by S. Boufi et al. [20] and D. PASQUINI et al. [21].

III.5 Analysis of morphology by optical microscopy

The micrographs of the composites (Figure 10) related to the incorporation of 5%, 10%, and 15% by mass of pistachio shell particles into the HDPE matrix clearly show a heterogeneous and irregular surface, as well as the presence of pistachio shell particle aggregates completely separated from the high-density polyethylene matrix. These aggregates increase in number with the rise in the percentage of pistachio shell powder incorporated into the HDPE matrix. This is due to the incompatibility of the two phases resulting

from the weak interfacial adhesion between the hydrophilic pistachio shell particles and the hydrophobic HDPE. These results are in good agreement with those reported by El-Shekeil et al [22], Al Maadeed et al [23], and Panaitescu et al [24].

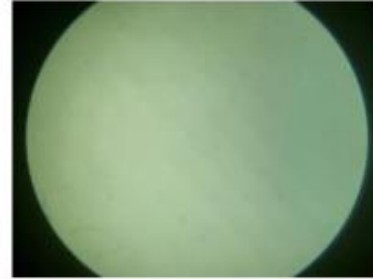


Figure 9: Optical microscopy micrograph of the Virgin HDPE surface.

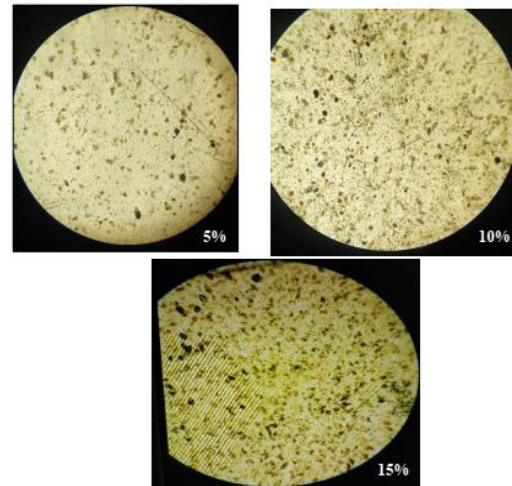


Figure 10: Optical microscopy micrograph of the surfaces of HDPE/PSF composites at different charging rates (5%, 10%, and 15% respectively).

IV Conclusion

This study aimed to develop and study filler/matrix composite materials, produced by conventional transformation processes (kneading followed by molding by compression). These composites consist of a high-density polyethylene matrix and Pistachio shell charge with dimensions less than 90 μm and rates varying 5%, 10%, and 15% by weight. The composites obtained are then characterized by determining the rheological properties, physical, mechanical, and morphological.

The analysis of the experimental results allowed us to draw the following conclusions:

- Rheological characterization by measuring the fluidity index made it possible to deduce that:
 - The HDPE/FCP composites fluidity index is decreased as a function of loading rate.
- The physical characterization by measuring the water absorption rate made it possible to deduce that :

- The increase in water absorption rate depends on the immersion time and the concentration of pistachio shell fillers.
 - The mechanical characterization of HDPE/FCP composites made it possible to deduce that there are:
 - An increase in the Shore D hardness of composites compared to the value of HDPE virgin.
 - A decrease in the resilience of HDPE/PSF composites with the increase in rate dump.

References

- [1] D. Verma, K.L. Goh, V. Vimal, Interfacial Studies of Natural Fiber-Reinforced Particulate Thermoplastic Composites and Their Mechanical Properties, *Journal of Natural Fibers*, 1-28, (2020).
- [2] L. Mohammed, M.N.M. Ansari, G. Pua, M. Jawaid, M.S. Islam, A Review on Natural Fiber Reinforced Polymer Composite and Its Applications, *International Journal of Polymer Science*, 243-947, (2015).
- [3] M. KOWALCZYK, E. PIORKOWSKA, P. KULPINSKI, & PRACELLA, "Mechanical and thermal properties of PLA composites with cellulose nanofibers and standard size fibers. Composites", Part A: Applied Science and Manufacturing, 42(10), 1509-1514, (2011).
- [4] K.Bledzki, O. Faruk, Creep and impact properties of wood fiber/polypropylene composites: influence of temperature and moisture content, *Composites Science and Technology*, 64, 693-700, (2004).
- [5] H. Demir, U. Atikler, D. Balköse, and F. Tihminlioğlu, "The effect of fiber surface treatments on the tensile and water sorption properties of polypropylene-luffa fiber composites," *Composites Part A: Applied Science and Manufacturing*, vol. 37, no. 3, pp. 447-456, (2006).
- [6] Xu. X. JAYARAMAN, K.C. MORIN, & N. Pecqueux, « Life cycle assessment of wood-fiber-reinforced polypropylene composites », *Journal of Materials Processing Technology*, 198(1-3), 168-177, (2008).
- [7] S.Th.Georgopoulos, P.A.Tarantili, E.Avgerinos, A.G. Andreopoulos, E.G. Koukios, Thermoplastic polymers reinforced with fibrous agricultural residues, *Polymer Degradation and Stability*, 90, 303-312, (2005).
- [8] A. BOURMAUD, & S. PIMBERT, «Investigations on mechanical properties of poly (propylene) and poly (lactic acid) reinforced by miscanthus fibers », *Composites Part A: Applied Science and Manufacturing*, 39(9), 1444-1454, (2008).
- [9] S.M.B. NACHTIGALL, G.S. CERVEIRA, S.M.L. ROSA, « New polymeric-coupling agent for polypropylene/wood-flour composites », *Polymer Testing*, 26: 619-628, (2007).
- [10] H. DEMIR, U. ATIKLER, D. BALKOSE, F. TIHMINGLIOGLU, « The effect of fiber surface treatments on the tensile and water sorption properties of polypropylene-luffa fiber composites », *Composites Part A: Applied Science and Manufacturing*, 37: 447-456, (2006).
- [11] M. KHALID, C.T. RATNAM, T.G. CHUAH, SALMIATON ALI, THOMAS S.Y. CHOONG, « Comparative study of polypropylene composites reinforced with oil palm empty fruit bunch fiber and oil palm derived cellulose », *Materials & Design*, 29: 173-178, (2008).
- [12] M. KACI, H. DJIDJELLI, A. BOUKERROU, L. ZAIDI, « Effect of wood filler treatment and EBAGMA compatibilizer on morphology and mechanical properties of low-density polyethylene/olive husk flour composites », *Express Polymer Letters*, 1: 467-473, (2007).
- [13] D. PASQUINI, E.M. TEIXEIRA, A.A. SILVA CURVELO, M.N. BELGACEM, A. DUFRESNE, « Surface esterification of cellulose fibers: Processing and characterisation of lowdensity polyethylene/cellulose fibres composites », *Composites Science and Technology*, 68: 193-201,(2008).
- [14] B. V. VOORN, H.H.G. SMI, R.J. SINKE et B. de KLERK, « Natural fibre reinforced sheet moulding compound». *Composites Part A: Applied Science and Manufacturing*, Vol.32, p 1271- 1279, (2001).
- [15] N.Stark, R.E.Rowlands, Effects of wood fiber characteristics on mechanical properties of wood/polypropylene composites, *Wood and fiber science*, 35, 167- 174, (2003).
- [16] N. PETCHWATTANA, et S. COVAVISARUCH, « Effects of rice hull particle size and content on the mechanical properties and visual appearance of wood plastic composites prepared from Poly(vinyl chloride) ». *Journal of Bionic Engineering*, Vol. 10, pp.110-117, (2013).
- [17] Y.T. ZHENG, D.R. CAO, D.S. WANG et J.J. CHEN, « Study on the interface modification of bagasse fibre and the mechanical properties of its composite with PVC ». *Composites Part A: Applied Science and Manufacturing*, Vol. 38, pp. 20-25, (2007).
- [18] M.N. ICHAZO, C. ALBANO, J. CONZÀLEZ, R. PERERA et M.V. CANDAL, « Composites Structures », Vol. 54, 207, (2001).
- [19] Badrina, D.; Hocine, D.; Amar, B.; Sébatien, M.; Ahmed, K. Morphological, mechanical, and physical properties of composites made with wood flour-reinforced polypropylene/recycled poly(ethylene terephthalate) blends. *Polym. Compos.*, 38 (8), 101-13, (2017).
- [20] S. BOUFI, M. ABDELMOULEH, M.N. BELGACEM, A. DUFRESNE, « Short natural-fibre reinforced polyethylene and natural rubber composites: Effect of silane coupling agents and fibres loading », *Composites Science and Technology*, 67: 1627- 1639, (2007).
- [21] D. PASQUINI, E.M. TEIXEIRA, A.A. SILVA CURVELO, M.N. BELGACEM, A. DUFRESNE,« Surface esterification of cellulose fibres: Processing and characterisation of low density polyethylene/cellulose fibres composites », *Composites Science and Technology*,68: 193-201, (2008).
- [22] Y.A. EL-SHEKEIL, S.M. SAPUAN, M. JAWAID et O.M. AL-SHUUJAA, « Influence of fiber content on

mechanical, morphological and thermal properties of kenaf fibers reinforced poly(vinyl chloride)/thermoplastic polyurethane poly-blend composites », *Materials and Design*, 58,130–135, (2014).

- [23] M. A. ALMAADEED, Z. NOGELLOVÀ, M. MICUŠIK, I. NOVÁK et I. KRUPA, « Mechanical, sorption and adhesive properties of composites based on low density polyethylene filled with date palm wood powder », *Materials and Design*, 53,29–37, (2014).
- [24] D. M. PANAITESCU, M. IORGA, Z. VULUGA, D. DONESCU, M. DAN, S. SERBAN et D. FLOREA, « L'effet de l'interface dans les composites de fibres naturelles et de matières plastiques », *Revue Roumaine de Chimie*, 52,409–414, (2007).

Comparative analysis of extracted chitosan versus commercial one: physicochemical effects of extraction

Aicha DEHANE^{*1,2}, Lisa KLAAL¹, Dalila HAMMICHE¹, Balbir Singh KAITH²

¹Université de Bejaia, Faculté de Technologie, Laboratoire des Matériaux Polymères Avancés Route De Targa- Ouzemmour, Bejaia 0600, Algérie

²Department of Chemistry, Dr. B.R. Ambedkar National Institute of Technology, Jalandhar 144 027, Punjab- India

Corresponding author*: aicha.dehane@univ-bejaia.dz

Received: 06 October, 2024; Accepted: 07 December, 2024; Published: 26 January, 2025

Abstract

This study successfully extracted chitosan from waste generated by local shrimp shells. Functional and physicochemical properties of Chitosan produced have been evaluated by several methods such as FTIR, XRD and DSC. The obtained chitosan showed similar physicochemical properties compared to commercial one prepared. Structure was confirmed by Fourier transform infrared spectroscopy; X-ray diffraction and differential scanning calorimeter have same differences to refer to the effect of methods of extractions and type of shrimp shells waste.

Keywords: Chitosan, Extraction, shrimp shells, Commercial chitosan.

I. Introduction

Chitosan, a linear polysaccharide generated from the partial deacetylation of chitin, has sparked widespread attention due to its many uses in biomedicine, pharmacology, and agriculture. Its distinct features, including as biocompatibility, biodegradability, and antibacterial activity, have made it an important material in a variety of applications. Chitin, the precursor to chitosan, is one of the most prevalent biopolymers on Earth, essentially extracted from crustacean exoskeletons, insect cuticles, and fungal cell walls [1]. Shrimp shells represent a significant source of chitin, largely because of their widespread use as a by-product of the seafood industry [2].

Chitosan utilized in industrial applications is predominantly sourced from crustaceans, particularly the shells of crabs, prawns, and shrimp, which are readily available as byproducts of the food processing industry. However, it is increasingly available as a side-stream.

A product derived from the breeding of cocoons within the silk industry, serving as a by-product of protein extraction from insects for food and animal feed industries, as well as fungal fermentation. Fish scales, composed of chitin, are frequently discarded due to their low yield, representing only 1 wt% of the total weight [3].

Chitosan is commonly extracted from shrimp shells using three steps: demineralization, deproteination, and deacetylation. In one research, chitosan was extracted from *Penaeus monodon* shells using an optimized method that included 1 N HCl for demineralization at 50 °C, NaOH for deproteination, and an alkaline process for deacetylation. The ultimate chitosan production was 82%, with outstanding physicochemical qualities [4]. The extraction of chitosan is conducted through a stepwise procedure that incorporates both acid and alkaline treatments, producing high purity and

yield [5]. The selection of reagents, temperatures, and reaction durations during extraction markedly affects the characteristics of the resulting chitosan. The application of concentrated NaOH at elevated temperatures increases the extent of deacetylation; however, it may also lead to a reduction in the molecular weight of chitosan [1]. Furthermore, the application of H₂O₂ for bleaching has demonstrated an enhancement in the whiteness and purity of chitosan, thereby rendering it more suitable for uses that necessitate elevated optical clarity, particularly within the pharmaceutical domain [6]. This research investigation outlines an enhanced protocol for the extraction of chitosan from shrimp shell waste, detailing each step and comparing the results with commercial methods. The objective is to demonstrate the effectiveness and reproducibility of this protocol in producing high-quality chitosan, while also suggesting its potential as a sustainable material for industrial applications.

II. Material and methods

II.1 Used biomass origin

The used shrimp shell waste for the extraction of chitosan was collected from Mers El phare port on the Mediterranean Sea, (Algeria). Commercial chitosan from shrimp shells 75% deacetylation Min 75% Ash 1.0% moisture 10.0% viscosity (1% solution) Min 200cpc from Loba Chemie Ltd 107.

II.2 Extraction of chitosan

The extraction procedure that is being used is a laboratory modification of the industrial procedure [7,8].

a) Demineralization

Shrimp shells were gathered, cleaned, and dehydrated. The dried shells were subsequently pulverized into a fine powder. Fifty grams of the resultant powder were hydrated in a 1 N

HCl aqueous solution, with continuous stirring for six hours at 50 °C. The liquid phase was subsequently removed, and the solid material was washed with distilled water until a neutral pH was achieved. The demineralized material was dried overnight at 50 °C and subsequently utilized in the next step without additional purification.

b) Deproteination

The dried, demineralized material was immersed in an 8% NaOH solution and continuously stirred at 80-100 °C for a duration of 6 hours. The solution underwent filtration, followed by multiple washes of the solid phase with distilled water until a neutral pH was attained. The deproteinized material was then dried overnight in an oven at 45 °C.

c) Bleaching

The dried, deproteinized material underwent bleaching by immersion in a 0.3% H₂O₂ solution with continuous stirring for a duration of 2 hours. The bleached material underwent filtration, followed by washing with distilled water, and was subsequently dried in an oven overnight.

d) Additional HCl Treatment

The bleached powder was subsequently incorporated into a 12.5 M HCl solution and stirred for 2 hours at a temperature range of 80-100 °C. Following treatment, the material underwent several washes with distilled water until a neutral pH was attained. The final product was dried overnight in an oven at 45 °C.

II.3 Fourier transform infrared spectroscopy (FTIR)

Infrared spectra of powders were obtained over frequency range of 400–4000 cm⁻¹ using a FTIR Spectra (Bruker alpha-P) (with KBr).

II.4 Thermal analysis ATG/DTG

Thermal analysis was carried out by a differential scanning calorimeter (Netzsch DSC-214 polyma) where 10 mg of the samples was put in the crucible with a heating.

III. Results and discussion

III.1 Fourier transforms infrared spectroscopy (FTIR)

Spectra resulting from FTIR analysis of chitosan samples are shown in Figure 1 in comparison with the commercial one; all the characteristic peaks of chitosan were detected in all samples at their specific wavelengths: 3490, 2971, 2910, 1643, 1552, 1421, 1022, 893 and 752 cm⁻¹. Several bands have been proposed as internal reference bands of chitosan: A peak at 3480 cm⁻¹ corresponds to the –OH stretching vibrations of water and hydroxyls, as well as the NH₂ stretching vibrations of free amino groups; Symmetric CH₃ stretching and asymmetric CH₂ stretching bands within 2971-2910 cm⁻¹; The amide I and amide II bands absorption bands in the chitosan spectrum were around 1643 and 1552 cm⁻¹, respectively. The ethylene group's scissoring band was also seen at 1421 cm⁻¹. The absorption bands around 1022 and 893 cm⁻¹ correspond to vibration C-O-C bonds, confirming monomer bonding via -glycosidic links. This result is in agreement with those found by different authors [9-14]. Certain variations in peak wavelengths are most likely caused by variations in natural sources and the extraction technique. The presence of a band stretching pattern in the extracted

chitosan that corresponds to the band stretching of commercial standard chitosan indicates that the extracted material is indeed chitosan.

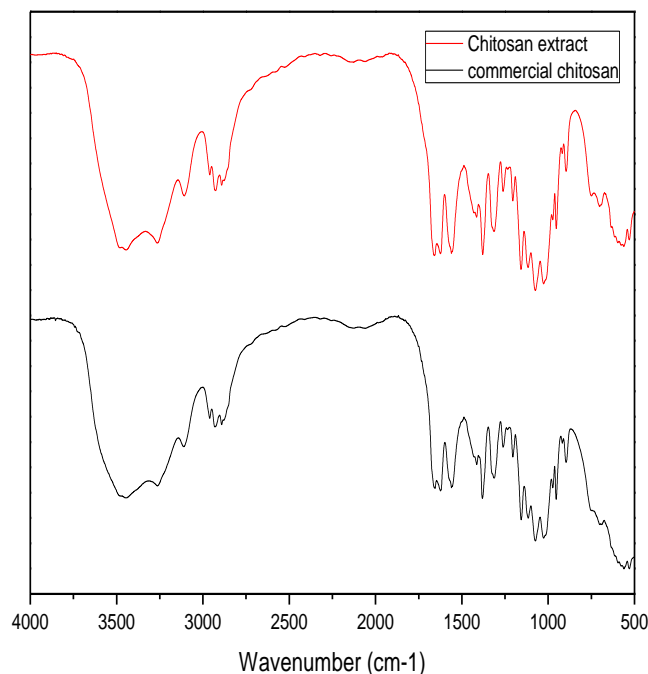


Figure 1: FTIR spectrum of the extracted chitosan and commercial chitosan

III.2 Thermal analysis ATG/DTG

The TGA curves of the Chitosan samples were plotted at two main stages of decomposition. The first was at 100 °C with a mass loss of 6.2% for Chitosan extracted and 12.5% for commercial Chitosan. Such loss is due to the evaporation of water molecules [15]. The second was variable, at 320 °C with a loss of 48.2% for Chitosan extracted, a loss of 49.2% for commercial Chitosan. This loss was caused by the depolymerization of the Chitosan chains [16]. Additionally, the details of the TGA are shown in the table below (Table 1)

Table 1: TGA Analysis results of extracted Chitosan and commercial Chitosan

TGA analysis	Extracted chitosan			Commercial chitosan		
	Temperature (°C)	100	320	650	100	320
Weight loss (%)	6.2	48.2	93.4	12.5	49.2	85.8

IV. Conclusions

In this study, chitosan was extracted from shrimp shell waste. The extracted chitosan was characterized. The results showed that the extracted chitosan had similar trends in the FTIR spectrum and TGA/DTG behavior compared to commercial chitosan indicating that extracted chitosan has comparable properties to commercial chitosan.

References

- [1] A. Pellis, G.M. Guebitz, G.S. Nyanhongo, Chitosan: Sources, Processing and Modification Techniques, 8 (7) 393, (2022).
- [2] T.K. Varun, S. Senani, N. Jayapal, J. Chikkerur, S. Roy, V.B. Tekulapally, M. Gautam, N. Kumar, Extraction of chitosan and its oligomers from shrimp shell waste, their characterization and antimicrobial effect 10 (2) 170–175 (2017)
- [3] P.K. Dutta, J. Dutta, V.S. Tripathi, Chitin and chitosan: Chemistry, properties and applications, Journal of Scientific & Industrial Research, 63, 20–31 (2004).
- [4] N. Boudouaia, Z. Bengharez, S. Jellali, Preparation and characterization of chitosan extracted from shrimp shell waste and chitosan film: Application for Eriochrome black T removal from aqueous solutions, Applied Water Science, (2019).
- [5] N. Kandile, H. Zaky, M. Mohamed, A. Nasr, Y. Ali, Extraction and characterization of chitosan from shrimp shells, Open Journal of Organic Polymer Materials, 8, 33–42 (2018).
- [6] R.S.C.M. de Queiroz Antonino, B.R.P.L. Fook, V.A. de Oliveira Lima, R.I.F. Rached, E.P.N. Lima, R.J.S. Lima, C.A.P. Covas, M.V.L. Fook, Preparation and characterization of chitosan obtained from shells of shrimp (*Litopenaeus vannamei* Boone), Marine Drugs, 15(5) 141 (2017).
- [7] M.S. Benhabiles, R. Salah, H. Lounici, N. Drouiche, M.F.A. Goosen, N. Mameri, Antibacterial activity of chitin, chitosan, and its oligomers prepared from shrimp shell waste, Food Hydrocolloids, 29(1) 48–56, (2012).
- [8] A. Abdulkarim, M.T. Isa, S. Abdulsalam, A.J. Muhammad, A.O. Ameh, Extraction and characterisation of chitin and chitosan from mussel shell, Civil and Environmental Research, 3(2) 108–114 (2013).
- [9] H. Helwati, S. Saleha, T. Iqbalsyah, Development of bioplastic from wheat Janeng starch for food packaging, in IOP Conference Series: Material Science Engineering, 012015 (2019)
- [10] A. B. Linares Veliz, J. C. Jiménez García, P. López, B. R. de Gásque, Biodegradability study by FTIR and DSC of polymers films based on polypropylene and Cassava starch, Electrons Journal Chemistry (2019)
- [11] K. M. Dang and R. Yoksan, Morphological characteristics and barrier properties of thermoplastic starch/chitosan blown film, Carbohydrate Polymer, 150, 40–47 (2016)
- [12] M.K. Rasweefali, S. Sabu, K.V. Sunooj, A. Sasidharan, K.A.M. Xavier, Consequences of chemical deacetylation on physicochemical, structural and functional characteristics of chitosan extracted from deep-sea mud shrimp. Carbohydrate Polymer. (2021)
- [13] N. Nawar Tamzi, M. Faisal, T. Sultana, S. Kumar Ghosh, Extraction and Properties Evaluation of Chitin and Chitosan Prepared from Different Crustacean Waste. Bangladesh Turkish Journal of Veterinary & Animal Sciences. 8, 69-76 (2020).
- [14] M.M. Mathaba, O. Daramola, Effect of Chitosan's Degree of Deacetylation on the Performance of PES Membrane Infused with Chitosan during AMD Treatment. Membranes. 10, 52 (2020).
- [15] D.D. Salman, W.S. Ulaiwi, A. Qais, Preparation of chitosan from Iraqi shrimp shell by autoclave, studying some physicochemical properties and antioxidant activity. Journal of Pharmaceutical Sciences and Research. 10, 3120–3123 (2018)
- [16] E.J. Dompeipen, M. Kaimudin, Isolasi Kitin dan Kitosan dari Limbah Kulit Udang. Majalah BIAM 092(1) 32–39 (2016)

Polymethyl methacrylate UV aging: numerical modeling and experimental validation

Aghilas HANNOU^{1,*}, Rabah FERHOUM¹, Marzak ZEROUKI¹, Madjid ALMANSBA¹

¹Laboratoire (LEC2M), Université Mouloud Mammeri de Tizi-Ouzou, Algérie.

Corresponding author*: aghiiii2013@hotmail.fr

Received: 15 October, 2024; Accepted: 02 December, 2024; Published: 27 January, 2025

Abstract

This work focuses on the experimental study and numerical modeling of the effect of UV aging on the macroscopic and microscopic behavior of Polymethyl Methacrylate (PMMA). The PMMA specimens, elaborated with the plastic molding process, were exposed to UV radiation in a chamber for two aging times: 120h and 250h. Thereafter, the specimens before and after exposures to UV radiation were visually analyzed and weighed on an analytical balance. Compression tests were carried out on the specimens with a strain rate of 10-3s-1. The effect of UV radiation on PMMA specimens was manifested at the macroscopic scale by: yellowing of the specimens, loss of mass, and decrease of some mechanical properties such as Young's modulus, and at the microscopic scale by breaking the c=O chains. UV aging was modeled by introducing mass loss into Young's modulus values. The model was implemented in the finite element code using the VUMAT subroutine. Simulations were conducted on PMMA specimens with different periods of exposure to UV radiation. Comparisons with experimental results demonstrated the capability of the implemented model to simulate the UV aging effect.

Keywords : Polymethyl Methacrylate (PMMA), UV aging, VUMAT, Abaqus/Explicit

I. Introduction

Due to their good specific mechanical properties and ease of processing, the application of industrial polymeric materials has considerably increased. The use of PMMA materials presents many advantages due to their low cost and their generally good mechanical properties, their low production cost, and their low density. They are used in all industry sectors, either as structural materials (aeronautics, cars, etc.) or as insulating materials (electronics and electrical engineering).

Plastics occupy a prominent place in our environment and are now present everywhere, PMMA is one of them. Since it is a completely amorphous polymer, its glass transition temperature is 105°C; this relatively high temperature allows it to work at a fairly high processing temperature [1] and thus has an exquisite visual appearance. Hence its major use outdoors, these materials degrade when exposed to temperature variations, rain or sunlight, and water or oils.

A wealth of literature has been reported on the degradation mechanisms of PMMA [2-5]. It is well recognized that ultraviolet (UV) irradiation causes significant physicochemical changes in polymers, resulting in a decrease in their mechanical performance through a drop in mass weights [6].

II.1 Background on photodegradation

Degradation of polymers significantly affects their mechanical behavior and the evolution of their microstructure. Two types of process can be distinguished, chemical (chain breaking) and physical (mass loss, and both strongly related). The degradation may be, for example, induced by physico-chemical attacks (water, oxygen, etc.), temperature, mechanical stress, and UV irradiation. The degradation mechanisms depend on the type of polymer (amorphous, semi-crystalline,...etc.) and the environment (temperature, chemical medium...etc.).

In general, these mechanisms are controlled by a variety of factors, including diffusion processes (e.g. diffusion of oxygen and/or water), the polymer morphology, and the concentration of impurities in the polymer.

In the last decades, many studies have reported that in many thermoplastic polymers such as polypropylene, polycarbonate, and PMMA, when exposed to Ultraviolet light, the primary structure undergoes considerable modifications due to chain scission and the creation of molecular defects such as carbonyl groups and crosslinking [7-9].

Polycarbonate (PC) subjected to UV irradiation shows important modifications in the optical properties by reducing its transparency and microhardness through the thickness proving a gradual deterioration in the depth [7]. Shyichuk et al., 2001; Craig et al., 2005 [10, 11] confirmed that when Polypropylene (PP) is exposed to UV radiation, the size of

the crystalline domains changes significantly, and chain scission events cause chain segments in the amorphous phase to become untangled, which improves crystallisability.

The mechanical characteristics of PLA decrease due to photodegradation. In particular, a loss of stiffness and strength was observed by S. Belbachir and al (2008) [12]. Ho and Pometto (1999) [13] and Ho et al. (1999) [14] demonstrate that prolonged exposure to UV light reduces the molecular weights and mechanical characteristics of PLA films, such as the young modulus, stress, and strain at break.

II.2 Scope of this work

This work is divided into two parts: the first part is experimental, which consists of studying the impact of aging by UV radiation on the behavior of PMMA. The second part is numerical which consists of modeling the effect of UV irradiation on the elastic-viscoelastic behavior of amorphous PMMA. A semi-phenomenological model able to capture the finite strain behavior of PMMA is elaborate to predict the photodegradation effect on the overall stress-strain response. Several models were elaborated and developed to describe the elastic-viscoelastic deformation of polymers [15-28]. In this study, the effect of degradation by UV radiation is introduced in Young's modulus as a function of mass loss. The model was implemented in the Abaqus/explicit finite element code using the VUMAT subroutine. Uni-axial compression simulations were conducted at different exposure times to UV radiation. The numerical results were compared with the experimental results.

The various experiments carried out in the present work have revealed the effect of UV radiation on the macroscopic and microscopic behavior of PMMA specimens. A loss of mass is observed after many hours under UV radiation. The degradation of the mechanical properties of PMMA such as the Young's modulus was noted. The comparisons between numerical predictions and experimental results demonstrated the capability of the implemented model to match the experimental results.

III. Results and discussion

III.1 Transparency

Figure 2 shows an increase in the yellowing aspect and a decrease in transparency of the irradiation PMMA, as the UV exposure time increase. This yellowing is the result of a chemical reaction caused by UV radiation. The UV energy absorbed by PMMA macromolecules generates a rupture of the most susceptible bonds, which can oxidize in the presence of oxygen. This mechanism is responsible for the formation of substances that cause the yellowing observed in the irradiation samples.

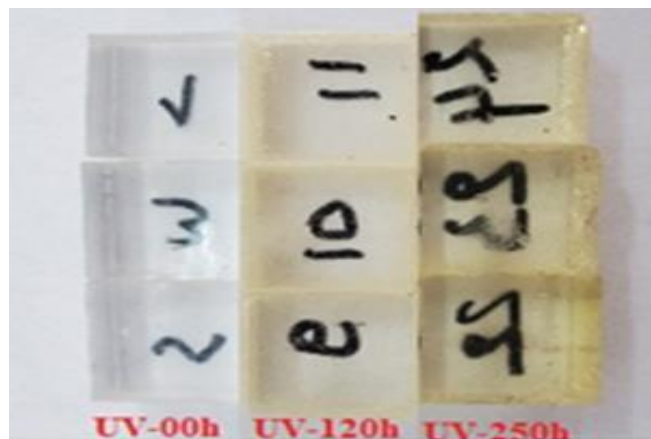


Figure 1: Transparency of the virgin and aged materials

II.2 Weighing measure

The evolution of mass loss as a function of UV exposure time is presented in Figure 2. The decrease in the mass of the specimens was observed with prolonged exposure to UV radiation. At 250h of exposure to UV radiation, the mass of the specimens was dropped from 1.11806g to 1.08534g (-0.03272g), equivalent to a loss of 3% of its initial mass. This loss of mass can be explained by the breaking of molecular chains.

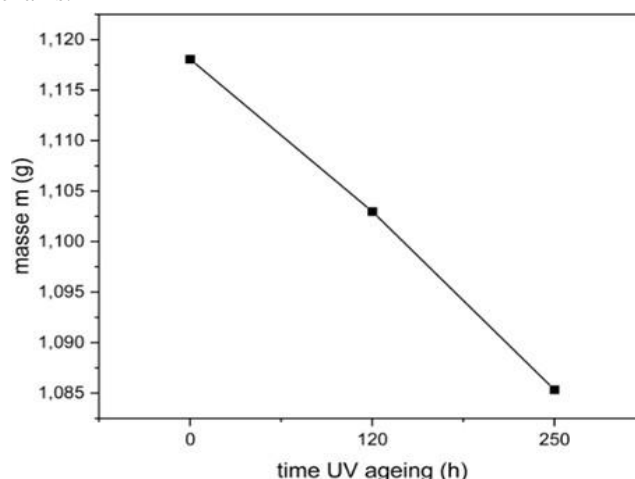


Figure 2: Mass evolution after UV irradiation.

It appears that most of the mechanical properties of PMMA have been affected by the degradation. Indeed, significant changes in Young's modulus (Figure 3).

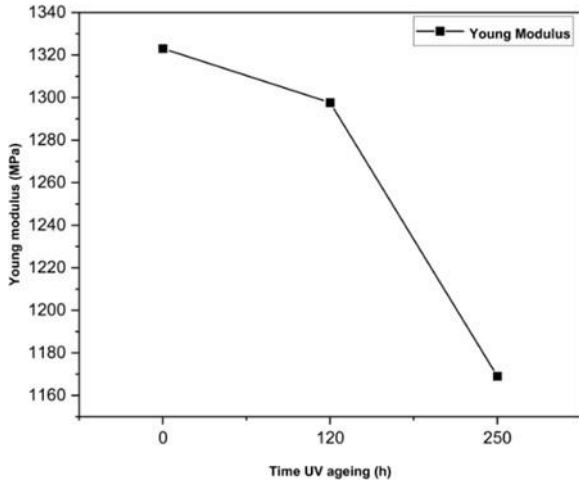


Figure 3: Young Modulus.

III.3 Numerical modeling

The isotropic and symmetric elastic behavior is a Hooke's law that is expressed as a function (1):

$$(1) \quad \sigma = E \cdot \varepsilon$$

Where σ the elastic stress tensor, ε the elastic strain tensor, and E the Young modulus.

The model developed by Tervoort [29] and modified by Mirkhalaf [26, 30] for thermoplastic materials is described in this section. The plastic strain rate tensor ε^{vp} is given by the equation (2):

$$(2) \quad \varepsilon^{vp} = \frac{\sigma^d}{2\chi}$$

Where σ^d the deviatoric part of the stresses is, χ is viscosity function 3 [26, 30-32] is given by:

$$(3) \quad \chi = \varphi_0 \exp\left(\frac{\Delta H}{RT} + \frac{\mu\sigma^h}{\sigma_0}\right) - \sigma_\infty^{soft} \left(1 - \exp\left(\frac{-h\sqrt{3}\bar{\varepsilon}^{vp}}{\sqrt{2}\sigma_\infty^{soft}}\right)\right) \times \left(\frac{\sigma^{eq}}{\sinh\left(\frac{\sigma^{eq}}{\sigma_0}\right)}\right)$$

The viscosity function depends only on the equivalent plastic strain $\bar{\varepsilon}^{vp}$ defined by equation (4):

$$(4) \quad \bar{\varepsilon}^{vp} = \int_0^t \sqrt{\frac{2}{3}} \varepsilon^{vp} : \varepsilon^{vp} dt$$

Where σ_0 is a material constant, R is the universal gas constant; T is the constant temperature; ΔH is the activation energy. φ_0 is a pre-exponential factor, is the pressure coefficient. σ_∞^{soft} is the softening parameter and h is The softening slope parameter.

III.4 UV aging equations of the model

Exposure of PMMA to UV radiation causes degradation of the mass and the values of Young's modulus (Figure 3 and Figure 4). This degradation was introduced into the numerical model by adding the effect of mass loss into Young's modulus. The law of Young's modulus degradation is expressed by the following equation (5):

$$(5) \quad E = E_0 - E_t$$

Where E is the degradation value of Young's modulus under UV radiation E_0 expresses the initial value of Young's modulus in the pristine state and E_t presents the value of Young's modulus as a function of the time of exposure to UV radiation and mass loss. It is expressed by equation 6:

$$(6) \quad E_t = E_0 \cdot \exp\left(-\frac{m_t}{m_0}\right)^{\frac{1}{n}}$$

m_t is the mass of the PMMA specimens after each exposure time to ultraviolet (UV) radiation, m_0 is the mass of the specimens without exposure to UV radiation, and n is a parameter depending on the exposure time of the specimens to UV radiation, it acquires values between 0 and 1. After substituting equation 6 into equation 5, we obtained equation 7:

$$(7) \quad E = E_0 \cdot \left(1 - \exp\left(-\frac{m_t}{m_0}\right)^{\frac{1}{n}}\right)$$

Young's modulus condition of the degradation and its implementation will be shown in the figure below (Figure 4).

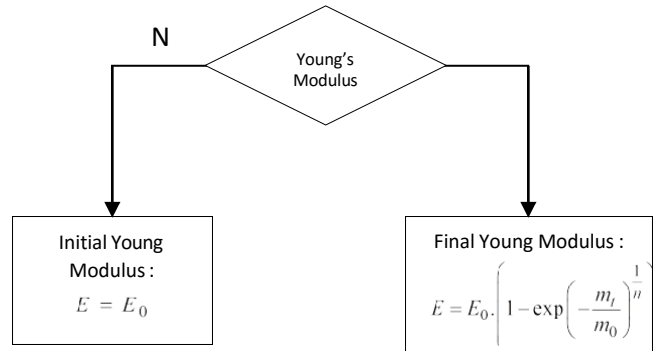


Figure: Diagram of the implementation conditions for the UV degradation

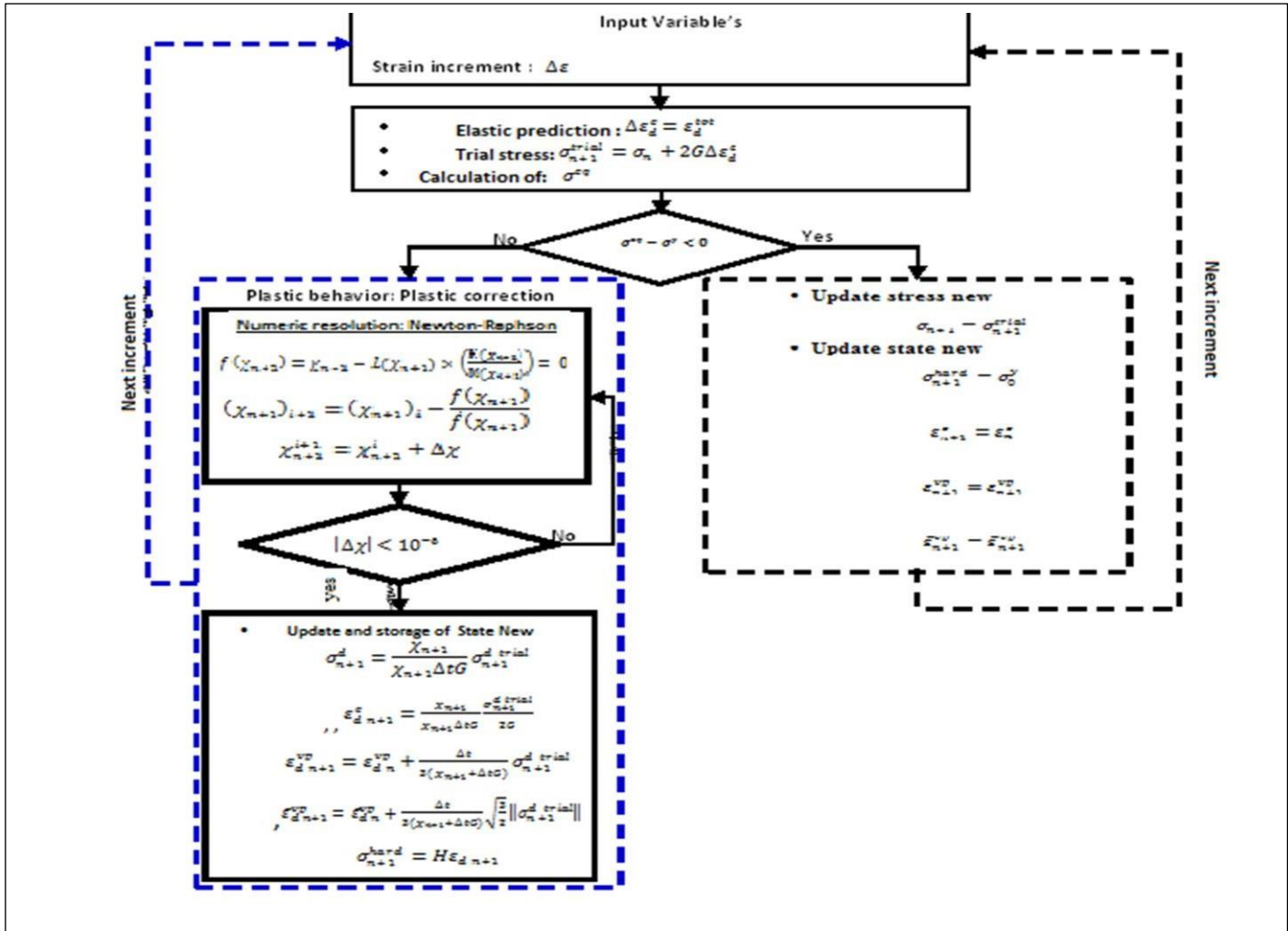


Figure 6: Organigram of the resolution model [31].

The model's equations were solved using the return mapping method. This method is described in detail in Mirakhalef's paper [26]. The model was implemented using the VUMAT subroutine in the Abaqus/Explicit well described in the following figure (Figure 6).

All the details of the development of this model, including the information, approximations, and adjustments to the equations used to ensure its performance in achieving our objective, are reported in the recently published article [31].

III.5 Mesh and Boundary Conditions

Figure 7 gives the boundary conditions imposed on the tested specimens (Dimension: 10x10x6 mm) in axial compression. Le maillage utilisé dans cette étude est de type C3D8R (3D finite element with reduced integration). The bottom rigid body has been fixed in the loading direction and an axial displacement of 2.5 mm has been imposed on the top rigid body.

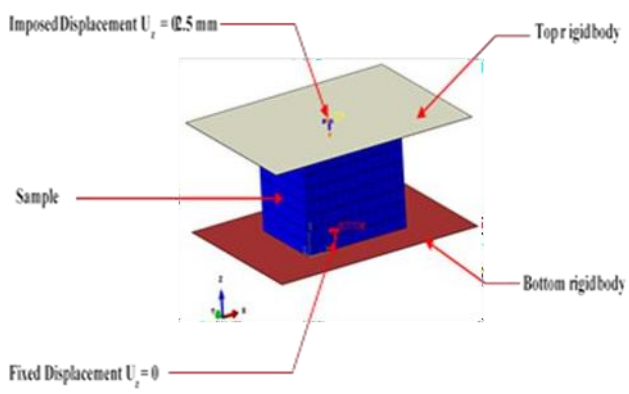


Figure 7: Boundary conditions were applied to the tested specimen

The material parameters used in this work have been listed in Table 1. The values of these parameters have been obtained after a parametric study [26, 30] and [32].

Table 1 Elasto-viscoplasticity model parameter's

E_0	ν	σ_0^y	H	σ_0	φ_0	σ_∞^{soft}	h	μ	ΔH	R	n
M	/	M	M	MPa	s				MJ		
Pa		Pa	Pa						$/mol$		
2200	0.4	1.95	4.6	00.6517	3.6e-25	29.7	8.0	0.010	3.e+08	8314.3	0.5

III.5 Numerical and experimental confrontation

In this section, comparisons between the experimental and numerical results have been carried out. Figure 8 illustrates the comparison between the numerical predictions and the experimental results for different exposure times to UV radiation. The implemented model correctly reproduced the behavior of the PMMA specimens under uniaxial compression and for the different UV exposure times. The divergence observed at the level of the maximum stress is explained by some limitations of the implemented model.

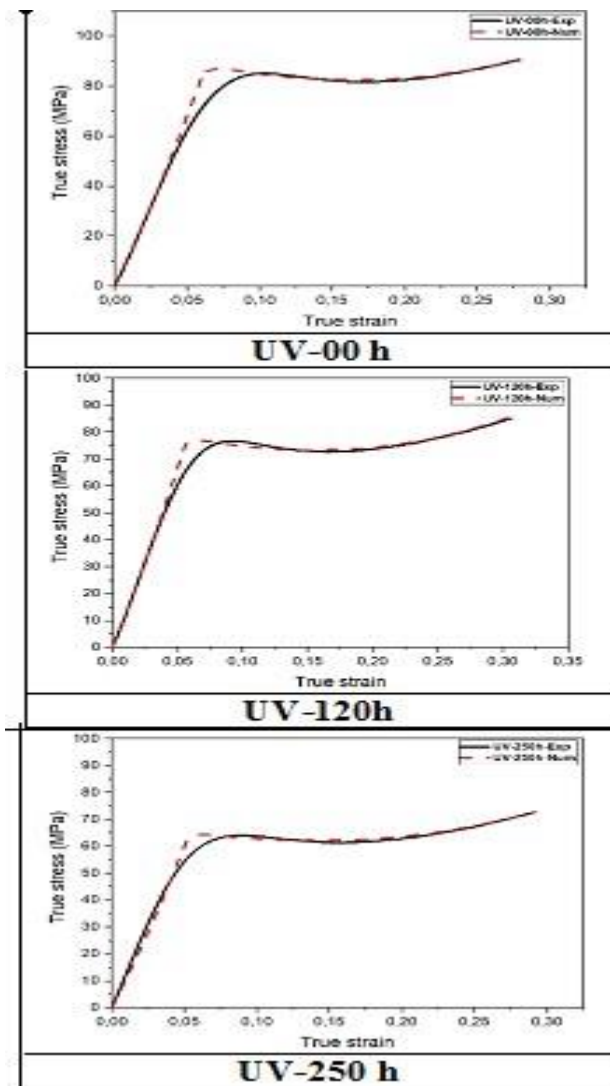


Figure 8: Comparison of true stress-true strain curves for each UV exposure time.

Figure gives the distribution of the von stresses in the PMMA specimens after deformation obtained with the implemented model. The deformation of the specimens is symmetrical and the maximum value of the stresses was reported at the thickness region. The result also shows a physical mesh deformation.

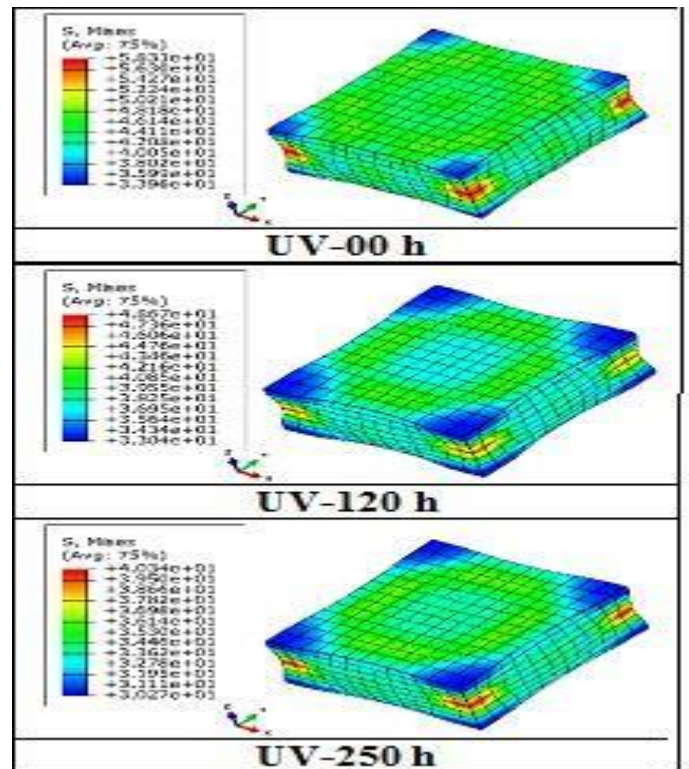


Figure 9: Von Mises stress distribution in the specimens after compression

Erreur ! Source du renvoi introuvable.-a shows the superposition of the true strain-true stress curves obtained by the implemented model. **Erreur ! Source du renvoi introuvable.**-b shows the superposition of the resulting experimental true strain-true stress curves. These superpositions have revealed the effect of the degradation of Young's modulus and the elastic limit introduced in the numerical model.

The comparison between the experimental and numerical degradation of Young's modulus is presented in **Erreur ! Source du renvoi introuvable.**-c. The results obtained show a good consistency between the experimental and numerical values. The degradation relation (equations 7) applied to Young's modulus gives a good prediction of the experimental data.

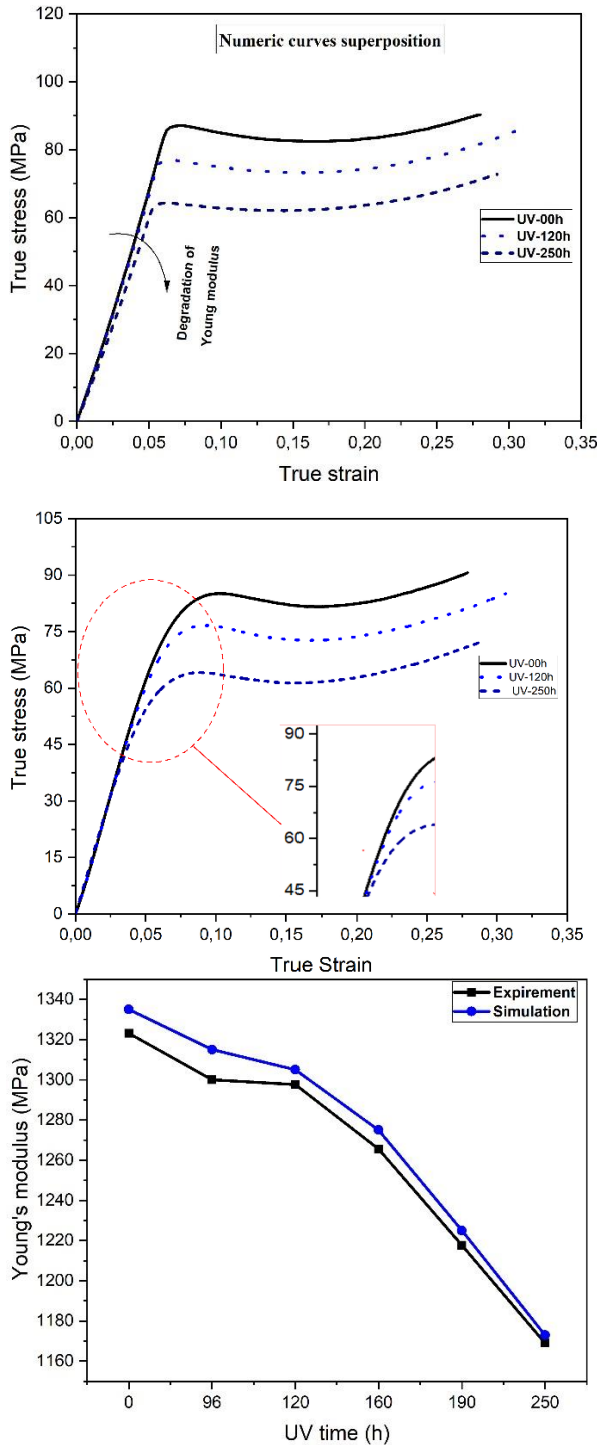


Figure 10: Comparing results for each holds time exposure: (a) numerical true strain-true stress curves, (b) experimental true strain-true stress curves, (c) numerical and theoretical degrading Young's modulus.

IV. Conclusions

Experimental investigations were conducted in this work concerning the effect of UV radiation on the macroscopic and microscopic behavior of PMMA specimens. These specimens were exposed to UV radiation for various hours: 120h and 250h. A series of tests were carried out on the specimens before and after exposure to UV radiation such as the uni-axial compression test. A loss of mass was observed on the

specimens exposed to UV radiation. Compression test results revealed that some mechanical properties of PMMA such as Young's modulus and yield strength dropped after exposure to UV radiation. The effect of degradation of Young's modulus was modeled by an exponential law as a function of mass loss. The modified model was implemented in the Abaqus/Explicit finite element code using the VUMAT subroutine. Simulations were carried out on PMMA specimens at different times of exposure to UV radiation. The numerical results obtained were compared with the experimental results. This comparison showed the ability of the implemented model to simulate the effect of Young's modulus degradation. In the future, we plan to extend the Tervoort model to take into account the maximum stress and to carry out experimental investigations on a wide range of polymers.

Nomenclatur

$\bar{\sigma}$: Stress tensor, $\bar{\epsilon}$: Strain tensor,
 E : the Young modulus
 $\dot{\epsilon}^v$: Rate of viscoplastic strain tensor,
 σ^d : Deviatoric part of the stress tensor,
 σ_0 : material constant,
 R : Universal gas constant,
 T : Constant temperature,
 μ : pressure coefficient,
 σ^{eq} : Effective or equivalent stress,
 σ^h : Hydrostatic stress tensor,
 σ_{ini} : initial yield strength,
 ν : Poisson's ratio,
 σ^{soft} : softening parameter,
 h : softening slope parameter,
 ΔH : activation energy,
 φ_0 : Pre-exponential factor,
 $\bar{\epsilon}^v$: Equivalent viscoplastic strain,
 σ^{hard} : Linear isotropic hardening,
 H : Hardening parameter,
 ϵ^d : Deviatoric strain,
 m_0 : mass of the specimens without exposure to UV radiation,
 m_t : mass of the PMMA specimens after each exposure time to ultraviolet (UV) radiation,
 n : parameter depending on the exposure time of the specimens to UV radiation, it acquires values between 0 and 1.

References:

- [1] N. Okhay, *Synthèse de réseaux polymères thermoréversibles par réaction de Diels-Alder*, Saint-Etienne (2012).
- [2] S. Li, The influence of the short-term ultraviolet radiation on the structure and properties of poly (p-phenylene terephthalamide) fibers, *Applied surface science*, 265, 519-526 (2013).
- [3] H. Tsuji, S. Miyauchi, *Poly (L-lactide): VI Effects of crystallinity on enzymatic hydrolysis of poly (L-*

- lactide*) without free amorphous region. Polymer degradation and stability, 71(3), 415-424 (2001)
- [4] G. Bae, T. Park, I.H. Song, *Surface Modification of Polymethylmethacrylate (PMMA) by Ultraviolet (UV) Irradiation and IPA Rinsing*. Micromachines, 2022. 13(11), 1952 (2022).
- [5] H. Tsuji, Y. Ikada, Properties and morphology of poly (L-lactide) 4. Effects of structural parameters on long-term hydrolysis of poly (L-lactide) in phosphate-buffered solution. Polymer degradation and stability, 67(1), 179-189 (2000)
- [6] H. Kaczmarek, L. Lindén, J. Rabek, Photo-oxidative degradation of poly (2, 6-dimethyl-1, 4-phenylene oxide) in the presence of concentrated hydroxy peroxide: The role of hydroxy (HO.) and hydroperoxy (HO₂.) radicals. Polymer degradation and stability, 47(2), 175-188 (1995)
- [7] S. Redjala, UV Aging Effects on Polycarbonate Properties. Journal of Failure Analysis and Prevention, 20(6) 1907-1916 (2020).
- [8] J. White, A. Shyichuk, Effect of stabilizer on scission and crosslinking rate changes during photo-oxidation of polypropylene. Polymer degradation and stability, 92(11), 2095-2101 (2007).
- [9] S. Redjala, Degradation of polycarbonate properties under thermal aging. Journal of Failure Analysis and Prevention, 19(2), 536-542 (2019)
- [10] A. Shyichuk, Quantitative analysis of the temperature effect on the radiation crosslinking and scission of polyethylene macromolecules. Journal of Polymer Science Part A: Polymer Chemistry, 39(10), 1656-1661 (2001).
- [11] I. Craig, Photo-induced scission and crosslinking in LDPE, LLDPE, and HDPE. Polymer Engineering & Science, 45(4), 579-587 (2005).
- [12] S. Belbachir, Modelling of photodegradation effect on elastic-viscoplastic behaviour of amorphous polylactic acid films. Journal of the Mechanics and Physics of Solids, 58(2), 241-255 (2010).
- [13] K.L.G. Ho, A.L. Pometto III, Effects of electron-beam irradiation and ultraviolet light (365 nm) on polylactic acid plastic films. Journal of environmental polymer degradation, 7(2), 93-100 (1999).
- [14] K.L.G. Ho, Degradation of polylactic acid (PLA) plastic in Costa Rican soil and Iowa state university compost rows. Journal of environmental polymer degradation, 7(4), 173-177 (1999).
- [15] S. Ahzi, Modeling of deformation behavior and strain-induced crystallization in poly (ethylene terephthalate) above the glass transition temperature. Mechanics of materials, 35(12), 1139-1148 (2003).
- [16] N.M. Ames, A thermo-mechanically coupled theory for large deformations of amorphous polymers. Part II: Applications. International Journal of plasticity, 25(8), 1495-1539 (2009).
- [17] L. Anand, N. Ames, On modeling the micro-indentation response of an amorphous polymer. International Journal of plasticity, 22(6), 1123-1170 (2006).
- [18] L. Anand, M.E. Gurtin, A theory of amorphous solids undergoing large deformations, with application to polymeric glasses. International Journal of Solids and Structures, 2003. 40(6), 1465-1487, (2003).
- [19] G.Ayoub, A continuum damage model for the high-cycle fatigue life prediction of styrene-butadiene rubber under multiaxial loading. International Journal of Solids and Structures, 48(18), 2458-2466 (2011).
- [20] G. Ayoub, Modelling large deformation behaviour under loading-unloading of semicrystalline polymers: application to a high density polyethylene. International Journal of plasticity, 26(3), 329-347 (2010).
- [21] D. Bochicchio, G.M. Pavan, Molecular modelling of supramolecular polymers. Advances in Physics: X, 3(1), 1436408 (2018).
- [22] M.C. Boyce, E.M. Arruda, Constitutive models of rubber elasticity: a review. Rubber chemistry and technology, 73(3), 504-523 (2000).
- [23] M.C. Boyce, D.M. Parks, A.S. Argon, Large inelastic deformation of glassy polymers. Part I: rate dependent constitutive model. Mechanics of materials, 7(1),15-33 (1988).
- [24] R. Haward, G. Thackray, The use of a mathematical model to describe isothermal stress-strain curves in glassy thermoplastics. Proceedings of the Royal Society of London. Series A. Mathematical and Physical Sciences, 302(1471), 453-472 (1968).
- [25] A. Makradi, A two-phase self-consistent model for the deformation and phase transformation behavior of polymers above the glass transition temperature: application to PET. International Journal of plasticity, 21(4), 741-758 (2005).
- [26] S. Mirkhalaf, F.A. Pires, R. Simoes, An elasto-viscoplastic constitutive model for polymers at finite strains: Formulation and computational aspects. Computers & Structures, 166, 60-74 (2016).
- [27] A. Adams, C. Buckley, D. Jones, Biaxial hot drawing of poly (ethylene terephthalate): measurements and modelling of strain-stiffening. Polymer, 41(2), 771-786 (2000).
- [28] R. Ferhoum, M. Aberkane, K. Hachour, Analysis of thermal ageing effect (hold time-crystallinity rate-mechanical property) on high density polyethylene (HDPE). International Journal of Materials Science and Applications, 2(3), 109 (2014).
- [29] T. Tervoort, A constitutive equation for the elasto-viscoplastic deformation of glassy polymers. Mechanics of Time-Dependent Materials, 1(3), 269-291 (1997).
- [30] S. Mirkhalaf, F.A. Pires, R. Simoes, Modelling of the post yield response of amorphous polymers under different stress states. International Journal of plasticity, 88, 159-187 (2017)

- [31] A. Hannou, Thermal Aging Effect on the Compression Behavior of Thermoplastic Polymers—Proposed Phenomenological Model. *Journal of Failure Analysis and Prevention*, (2023).
- [32] A. Hannou, R. Ferhoum, M. Almansba, Thermal aging effect on the mechanical behavior of polycarbonate: Experimental and modeling. *Materials Today: Proceedings*, 53, 202-208 (2022).